APPLICATION OF SPECTRAL SHAPING FOR SIMULATING NUCLEAR WEAPON ENVIRONMENTS

PROSPECTUS

Nicholas J. Quartemont, First Lieutenant, USAF

AFIT-ENP-MS-19-M

DEPARTMENT OF THE AIR FORCE
AIR UNIVERSITY

AIR FORCE INSTITUTE OF TECHNOLOGY

Wright-Patterson Air Force Base, Ohio

AFIT-ENP-MS-19-M

Application of Spectral Shaping for Simulating Nuclear Weapon Environments

PROSPECTUS

Presented to the Faculty

Graduate School of Engineering and Management

Air Force Institute of Technology

Air University

Air Education and Training Command

in Partial Fulfillment of the Requirements for the

Degree of Master of Science in Nuclear Engineering

Nicholas J. Quartemont, BS

First Lieutenant, USAF

March 2019

AFIT-ENP-MS-19-M

Application of Spectral Shaping for Simulating Nuclear Weapon Environments

Nicholas J. Quartemont, BS
First Lieutenant, USAF

Approved:

Capt James E. Bevins (Advisor)	Date
Dr. James C. Petrosky (Member)	Date
Dr. Abigail A. Bickley (Member)	Date
Lt Col Michael B. Shattan (Member)	Date

Table of Contents

Page

List of Figures

List of Tables

1. Introduction

1.1 Motivation

Nuclear deterrence is the cornerstone of U.S. nuclear policy and strategy [1]. There are many crucial aspects that contribute to the impact of nuclear deterrence, such as deterring nuclear and conventional threats and protection of allies. Two key attributes related to nuclear deterrence credibility are deterrence through attribution and the surety of nuclear weapon systems to function if needed.

A key strategy under countering nuclear terrorism in the 2018 Nuclear Posture Review affirmed the importance of "deterring state support for nuclear terrorism through advanced forensics and attribution capabilities" [1]. To this end, the technical nuclear forensics (TNF) community requires the ability to general representative post-detonation debris samples for training and development of attribution techniques. The generation of accurate fission product inventories in the representative debris is both extremely important for the attribution of the origin of a nuclear device and very difficult to do with existing facilities.

Additionally, an important nuclear weapon testing related mission is radiation effects on electronics in nuclear systems. The current neutron sources do not have an accurate energy or temporal distribution for the nuclear environment that nuclear systems are required to survive in certification testing. This problem is complicated further as the transmitted neutron flux through the physical environment and to the target varies significantly in energy and temporal distribution depending on the

scenario and system being considered. To address this capability gap, it would be beneficial to have a testing capability with an accurate temporal profile.

The final full scale U.S. nuclear weapon testing, code named Divider, was performed on 23 September 1992. The non-proliferation of nuclear weapons and general health concerns from the radioactive emissions were key drivers for eliminating testing of any kind. The Comprehensive Test-Ban Treaty (CTBT) banned nuclear explosions for all signatories or supporting nations for an indefinite duration since 1996. A handful of tests have been conducted after the CTBT's effective date; none have been by the U.S. However, there is still a need for the capabilities previously provided through nuclear testing for the study of environments to enable nuclear deterrence and non-proliferation through nuclear weapon certification and attribution of the origin of a nuclear detonation.

Each U.S. administration has supported the requirement and maintenance of a nuclear force structure after the elimination of nuclear tests. President Donald Trump stated at the 2018 State of the Union Address, "As part of our defense, we must modernize and rebuild our nuclear arsenal, hopefully never having to use it, but making it so strong and powerful that it will deter any acts of aggression" [2]. The National Nuclear Security Admnimistration (NNSA) is tasked with the mission of maintaining the nuclear stockpile's safety, security, and effectiveness under the Stockpile Stewardship Program (SSP).

Representative nuclear weapons system and effects testing is carried out through various organizations in the Department of Energy (DOE), Department of Defense (DOD), and supporting organizations. The scope of the testing sites is incredibly wide, ranging from radio frequency communications to the prompt gamma and neutron emissions following a nuclear event. A summary of some of the nuclear weapons effects testing simulation and facility capabilities is shown in Table 1. Testing is con-

ducted on components of the nuclear weapons themselves and the effects on targets. Near system level tests such as hydrodynamic testing are also performed with inert pits, such as U-238 [3]. Many aspects of nuclear weapons are only available for testing via computational methods or small-scale experiments, which may not truly represent the physics of the nuclear weapon.

Previous work has shown that there is a capability gap to reproduce nuclear weapon effects (NWE) of interest to national security applications [4, 5]. A key consideration for testing is the neutron energy spectrum in comparison with the environment that a nuclear weapon would see or produce. A particular spectrum of interest is the combination of a thermonuclear (TN) and prompt fission neutron spectrum (PFNS) as the present testing does not address this region to a large extent. The vast majority of testing facilities are focused on the Watt-fission spectrum, while a few are capable of producing the 14.1 MeV TN component from the deuterium-tritium (DT) fusion process [6]. The current prompt neutron facilities available are not well suited for the TN+PFNS application testing because of the lack of high energy neutrons, or there is not a large enough flux of neutrons on target. Several examples of testing facilities for prompt neutrons outlined in Table 1 are the Sandia Pulsed Reactor III (SPR), Sandia Annual Core Research Reactor (ACCR), White Sands Missile Range (WSMR) Fast Burst Reactor (FBR), the Los Alamos National Laboratory (LANL) Rotating Target Neutron Source (RTNS), and the LANL Weapons Neutron Research facility (WNR). The differential spectral profile of these sources compared to a notional TN+PFNS is shown in Figure 1.

Each of the available neutron sources has an important purpose for national security applications; however, they cannot meet the energy spectrum of every nuclear testing requirement. In comparison with the TN+PFNS, nearly all of the neutron sources are heavily weighted to lower energies and do not contain enough high energy

Table 1. U.S. nuclear weapons effects testing simulators and facilities [4]

Nuclear Weapon Environment	Test Facilities	Comments
Prompt and modified neutron	Sandia Pulsed Reactor III (or equivalent)* Annular Core Research Reactor White Sands Missile Range Fast Burst Reactor (also combined gamma) Los Alamos Neutron Science Center, Ion Beam Laboratory, and Rotating Target Neutron Source	For nuclear warhead subsystem space simulations For nuclear warhead components For ground systems, satellites, and interceptors For component tests and model validation
Prompt cold X-rays (plasma radiation source)	Upgraded Saturn and/or Double Eagle National Ignition Facility and/or Z-Refurbished (ZR)	For space system components/optics For future re-entry vehicle/re-entry body (RV/RB) material and interceptors
Prompt warm/hot X-rays (Bremsstrahlung source)	Upgraded Saturn and/or Pithon Modular Bremsstrahlung Source	For medium-dose electronics and cables For hardness surveillance and low-dose boxes
Prompt gamma	High-Energy Radiation Megavolt Electron Source (HERMES) III Pulserad (1150 or 958)	High dose-rates for strategic systems Low dose-rates for satellites and interceptors
Electromagnetic pulse	White Sands Missile Range Horizontally Polarized Dipole (HPD) Facility (2nd generation) Naval Air Warfare Center HPD Facility, Vertically Polarized Bounded Wave	For Army systems For aircraft and missiles
Source region electromagnetic pulse	HERMES III	For Army vehicles and field command, control, and communication systems
Impulse	Light Initiated High Explosive (LIHE) at Sandia National Labs Flyer-plate (magnetic or LIHE)*	For RV/RB internal components/mounts For future RV/RB aeroshells
Blast and shock	Large Blast Thermal Simulator Sandia National Laboratory Thunder Range	For ground vehicles, structures, non-ideal air blast (NIAB) simulations For RV/RB systems
Disturbed atmospheric radio frequency/infrared/ visible	Communication Chanel Scintillation (Wide-band Channel Simulator) Optical background (Nuclear Optical Dynamic Display System)	For military satellite communications, interceptor in-flight communications, and seekers

*Not currently available.

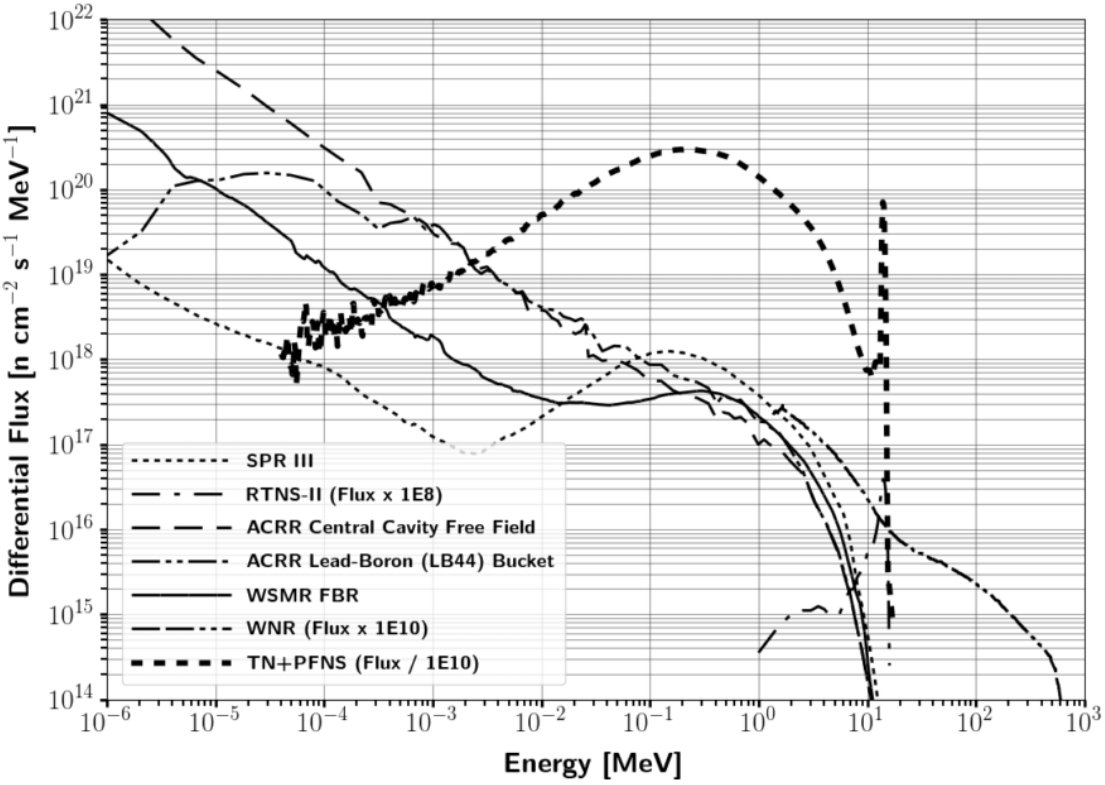

Figure 1. Comparison of selected neutron sources to notional TN+PFNS [5]

neutrons for the TN component. The RTNS has a high energy component, but the magnitude of the flux is substantially lower than required for some applications. The temporal aspect of the neutron flux also does not generally match to a nuclear weapon spectrum. Additionally, these large facilities often go underfunded or are shutdown. For example, the SPR-III was decommisioned in late 2006. Gathering accurate experimental results requires a neutron flux spectrum equivalent to that of a true nuclear event, which creates a need for a neutron source capable of emulating the environment. Therefore, development of a TN+PFNS source would enable production of the correct fission product inventory in surrogate debris and thereby enhance the ability of the TNF community to perform the attribution mission.

1.2 Background

Many approaches can be used to create nuclear weapon relevant neutron spectra in the absence of full-scale nuclear weapons testing. Some mechanisms are more applicable within different communities in nuclear sciences. Four main possible ways that the neutron environments are approximated for synthetic fission product debris production are sample doping, direct production using fission converters, surrogate methods, and spectral modification of existing sources [5]. In the context of neutron effects on electronics, the key approaches utilized are using existing source, computational models, and surrogate charged particle reactions. Each of these methods are limited in representing the neutron environment experienced in a nuclear weapon.

The sample doping technique irradiates with sources to build up a sample that is subject to a desired energy dependent fluence for the application, but the process is time and/or manpower intensive and the neutron fluence is not prompt requiring several corrections to the sample. A somewhat common TNF application using sample doping is the production of glass surrogate fallout debris for use in exercises or training [7]. The glassy matrix is created to emulate the solidified fission debris and entrained environment that is swept up in the stem of a nuclear explosion. The glass is doped with uranium and irradiated under various neutron environments depending on the requirements; however, the irradiation often done with a thermal neutron reactor. Additionally, the sample doping technique can be approached by irradiating different samples at different facilities. A final sample which has the "correct" fission product ratios can be created by selectively pulling mass chains from the irradiated samples. This sample doping technique creates a fission product debris sample; however, the spectral and temporal nature of the sample is not equivalent to what would be produced in a real nuclear explosion.

Direct conversion utilizes nuclear reactions to create a shaped neutron flux, which

can be done via charged particle interactions or through fusion sources with a fission converter. It has been shown that direct production is "impractical, complex, and unlikely to be implemented for safety or technological limitations" [5].

Surrogate methods rely on the formation of an equivalent compound nucleus through an alternative reaction mechanism [8, 9]. Surrogate methods are popular in studies where forming the product nucleus through the desired reaction is difficult or the energy cannot be fine-tuned. An example of this is neutron induced fission on U-235. A possible surrogate for U-235 neutron induced fission reaction, (n,f), is Th-232 (α,f), where the U-236 compound nucleus is formed. The surrogate reaction is useful for studying the fission products from 14 MeV neutron induced fission. The fission process is a function of the compound nucleus and independent of formation; however, the nucleus retains momentum, energy, spin, and parity [10]. A 25.6 MeV α particle provides the same excited state U-236 as a 14 MeV neutron in this example [10]. The surrogate approach has seen success; however, the nuclear data supporting the reactions is not as well understood [10, 11]. Additionally, there are some assumptions on the compound nuclear equilibration and spin-parity state which can impact the decay channels of the studied reactions [8].

Another commonly used surrogate method is to utilize charged particles for neutron damage in radiation effects on electronics. Ion beams can be used as a surrogate for neutrons by comparing the relative displacements per atom caused by the charged particle compared to a neutron [12]. A major benefit of using ion beams is that the energy can be finely tuned both in energy and deposition location, whereas neutrons are not as easily controlled. A disadvantage of using charged particles is that a large portion of the energy deposition as it travels through materials is based on electronic stopping power, while the neutral neutrons have negligible interactions. The Qualification Alternatives to the Sandia Pulsed Reactor (QASPR) program is the most

significant venture into the use of surrogate ions to perform neutron effects component level testing as a replacement alternative for the SPR [4]. QASPR combines operational irradiation facilities with modeling to predict neutron effects. While there have been substantial improvements to increasing the verification and validation of simulated data to experimental outcomes, the validation for the experimental data benchmarked to neutron experimental data is lacking in many cases [13].

The final approach that could be used is spectral modification, a method of altering a neutron spectrum through nuclear interactions to generate an energy spectrum of interest. Fundamentally, spectral modification is the goal of water moderated nuclear reactors to increase efficiency and allow the use of low enriched fuel.

Spectral modification is also performed in beam shaping assemblies used for boron neutron capture therapy (BCNT) where a neutrons are used to treat tumors through neutron capture reactions in boron. A somewhat optimized objective neutron spectrum focused on the epithermal region is published by the International Atomic Energy Agency (IAEA) [14]. BCNT has been explored with a wide variety of sources including accelerators and deuterium-deuterium (DD) fusion. A beam shaping assembly can be designed to moderate a source neutron flux to appropriate thermal, eipthermal, and fast spectrum for BCNT [15]. The build up of a design is produced primarily through moderation, reflection, and collimation of neutrons to the patient [16]. However, the approach to designing a beam shaping assembly lends itself to inefficiencies from an energy and population perspective.

A novel approach spectral modification approach was developed by the University of California-Berkeley and Lawrence Livermore National Laboratory (LLNL) for the development of an energy tuning assembly (ETA) to modify the National Ignition Facility (NIF) source to produce a TN+PFNS [5]. To perform the spectral modification, the Coeus metaheuristic optimization software package was developed to avoid

manpower intensive iterative studies and enable the rapid design of future ETAs to convert a facility's characteristic source spectrum to any arbitrary objective spectrum, within the constraints of physics [17]. Gnowee, the Coeus opimization engine, was developed for "rapid convergence to nearly globally optimum solutions" of this class of engineering problems [18]. It is important to note that the Gnowee and Coeus codes have applicability over a wide range of engineering problems, not just for the production of a TN+PFNS.

The result of the ETA design produced an acceptable representation of the TN+PFNS with the associated fission product distribution. The ETA design has been built and preliminary validation tests were conducted at the Lawrence Berkeley National Laboratorys 88-Inch Cyclotron [5, 19]. The preliminary validation utilized 33 MeV deuterium breakup on tantalum as a neutron source and investigated the ability to model the ETA performance [19]. Integral validation is planned in fiscal year (FY) 2019, and a development shot to enhance ETA performance is planned in FY2020.

1.3 Problem

The previous work made great progress; however, there are several deficiencies that need to be addressed. The broad research objective for this work is *Can an accurate neutron energy distribution expected from a "typical" thermonuclear or boosted nuclear weapon detonation be produced using spectral modification at the NIF?*. This research effort aims to address three main problem areas for ETA and spectral shaping of neutron sources for simulating nuclear weapon environments that were raised by previous work. Each are detailed below, organized by the experiment supported), along with accompanying research objectives. The enhanced ETA is referred to as "A THErmonuclear and prompt fission Neutron spectrum energy tuning Assembly" (ATHENA) for differentiation from the original ETA.

1. FY 2019 NIF shot (ETA): Systematic uncertainty is not fully addressed in the previous ETA calculations
    - Quantify the impact of nuclear data covariances of the simulated results for the neutron energy spectrum, foil activation rates, and fission product production rates
    - Design a foil activation diagnostic pack to provide better resolution in the epi-thermal neutron energy range
    - Prioritize and estimate production of fission products for radio-chemical analysis using recently published data
2. FY 2020 NIF shot (ATHENA): The current ETA efficiency is too low for use as a production NTF and NWE source
    - Develop a more representative neutron spectrum
    - Update facility constraints to reflect recent NIF upgrades
    - Develop a new ETA design to increase the ETA efficiency to produce $\sim 10^{12}$ fissions
3. FY 2020 NIF shot (ATHENA): The ETA at NIF was not evaluated for use as a 'short pulse' neutron source (SPNS)
    - Model the neutron timing profile and expected flux
    - Incorporate the ability to measure the neutron time profile into the FY 2020 ETA design

1.4 Questions and Hypothesis

The research questions and hypotheses associated with the problems outlined in Section 1.3 are detailed below. They are organized by the problem and capability

that they support.

1. 2019 ETA Fission Product Experiment

    - **What is the impact of nuclear data covariance on the simulated results?** It is expected that including nuclear data uncertainty will increase the relative error by approximately 1% for integrated and well understood reactions and may extend over 10% for less studied reactions thereby dominating Monte Carlo statistical uncertainty.
    - **Does the activation foil pack have sufficient coverage of the neutron spectrum to be used for unfolding?** It is expected the current design is not sufficent to robustly unfold the neutron spectrum should the model deviate from experimental results. The nuclear data covariance error will be used in lieu of radiation counting statistics to determine the activities associated with each foil. The unfolded results will indicate if the foil diagnostic pack is acceptable to unfold the ETA generated neutron spectrum.

2. 2020 ATHENA Surrogate Debris Experiment

    - **Can the ETA efficiency be increased to achieve $10^{11} - 10^{12}$ fissions?** This will be a factor of 100 to 1000 over the original ETA design. The gain will be possible due to NIF source development, changes to the design envelop, updated TN+PFNS objective spectrum, and changes to the optimization objectives.
    - **How well does the enhanced ETA perform to match the objective neutron environment?** The chi-square statistic will be used similarly to the goodness of fit criteria for the original ETA design.

3. 2020 ATHENA SPNS Experiment

- **Can an ETA-SPNS be useful as a capability for testing of prompt neutron environments?** The original ETA design has a pulse length on the foils of approximately 1 ms for neutrons in the range of XX to YY MeV. It is anticipated that this can be optimized with Coeus and assessed against an objective spectrum and fluence.

1.5 Assumptions and Limitations

An omnipresent limitation in many studies of science and engineering is the quality and quantity of available data for applications. Nuclear engineering commonly draws from published works containing the relevant nuclear data and the uncertainties behind them. The results presented are limited by the currently accepted understanding of nuclear physics phenomena and by the limitations of published data that is consistently being improved upon by the nuclear science community.

The second limitation, which is done so for convenience and publishing ability, is that the nuclear weapon environments are presented at an unclassified level. All information used to develop the neutron flux and profile is available in open literature or derived from unclassified information to produce a representative environment. The accuracy of the representative neutron environment compared to a specific real-world nuclear weapon scenario was not analyzed and will not be presented. The scope of this work aims to provide a position where, if desired, one could easily go from the unclassified spectrum to one that fully meets a requirement.

An assumption for this work is the choice of the NIF as the neutron source. Other sources may be present that would also perform the role, but NIF has unique benefits such as the prompt nature of the neutron yield and the fast neutrons arising from DT fusion. Although the NIF has been in operation since approximately 2010, there

is a potential insertion of systematic error based on the source characterization and variability in the source output.

Nuclear weapons can be categorized into three general classes: fission, boosted and TN [6, 20]. It has been shown that the majority of the present capability to produce synthetic debris is most focused on the fission devices [5]. The TN+PFNS was chosen in previous work because it is an area that lacks substantial source development. It is important to note that there is not just one spectrum that can classify the TN+PFNS. The TN portion of the weapon spectrum is assumed to be pure DT fusion [20]. The impact of weapon design, which can vary substantially and play a large role in the resultant neutron energy spectrum, is not evaluated in this work.

Some physical phenomena present in a true nuclear event are not taken into consideration for this analysis. First, the temperatures seen in nuclear weapons are on the order of 10^7 K, which is not feasible for the experiment [21]. Second, the time dependency of the internal neutron flux as the weapon is configured is not taken into account. Additionally, there will be large changes to the flux from initiation to burnout, and this work looks at a time and volume average result. Third, the synthetic weapon debris is created without induced fractionation. It is feasible to perform some level of fractionation; however, the levels of refractories and volatiles will not be altered in this work.

1.6 Approach

The spectral shaping problem is defined by the objectives and constraints. For this research, the problem objectives are the ETA spectrum for fission product generation and ATHENA spectrum for enhanced fission product generation and SPNS. The problem constraints are based on the NIF source term and mechanical envelope. The input objectives and constraints are utilized in Coeus to produce a nearly-globally

optimum solution for an ETA. The work performed previously has a completed design for the original ETA that will be used for all analysis of the expected experimental performance.

Coeus is used as an optimization tool to develop ATHENA [18]. The constraints for the problem are governed by the NIF source which is modeled as the polar direct drive exploding pusher (PDXP), stay-out angle defined by the incident lasers to drive the fusion, and the constrains of the NIF Target and Diagnostic Manipulator (TANDM). The objective spectrum for ATHENA is an improved TN+PFNS with the goals of increasing the number of fissions in the HEU sample and better representing the neutron environment. The ATHENA objective spectrum is also appropriate for neutron effects on electronics testing for high altitude burst or space environments. The neutron energy distribution is modified by the atmosphere; however, negligible attenuation occurs in a near vacuum.

The point designs are modeled with MCNP and SCALE version 6.2 to perform neutron radiation transport. MCNP is used for continuous energy solution, while SCALE is used for group-wise covariance analysis. MCNP versions 5 and 6 are both used depending on compatibility with surface source read (SSR) files generated by the NIF and LLNL. Utilizing two different radiation transport models also increases the degree of confidence in the results. The radiation transport simulations provide results for the reaction rates for foil activation, neutron energy spectra, and temporal aspect of the neutron flux.

A General Description of Fission Observables (GEF) is utilized for developing the expected fission product yields. GEF is a Monte Carlo and theory based approach that incorporates experimental data to determine fission observables, such as fission products [22]. Empirical methods for determining fission product distributions also exist. A formulation of this fit by S. Nagy would be beneficial for comparison to

GEF [23]. These empirical methods often include simplifications, such as ignoring neutron multiplicity, to create a simpler equation and more direct tie to existing data - both a benefit and limitation of this approach.

A foil pack designed to be placed in the ETA experimental cavity will be created to be able to successfully unfold the incident neutron spectra from the activation foils. The activation foils are selected with many important factors including the confidence in the nuclear data and energy range that the foils are activated. The modeled foil activities are used with the underlying nuclear data to unfold the neutron spectrum using Pacific Northwest National Laboratory (PNNL) STAYSL. STAYSL relies on least-squares spectral adjustment based on the chi-squared of the measured activities to determine the incident neutron flux [24]. The nuclear data-covariance uncertainty is used as the activation uncertainty in the unfolding, which will provide a higher level of confidence in the spectral agreement. The true activation uncertainty will almost certainly be below that of the nuclear data covariance sampled values.

2. Theory

2.1 Neutron Interactions with Matter

Neutron interaction mechanisms with matter serve as a physical constraint to spectral shaping of a neutron flux spectrum. Neutron interactions can act to moderate, absorb, or even emit more neutrons. The major reaction mechanisms available in the range of the fast to thermal energies that are relevant to nuclear weapon environments are elastic scattering, inelastic scattering, radiative capture, and the release of 'x' particle (n,xn) reactions. Fission reactions are an extremely important reaction mechanism for the formation of synthetic weapon debris; however, fission does not contribute largely to the spectral modification problem for this application. A diagram summarizing the important neutron reactions is shown in Figure 2.

The neutron interaction probability is described by the neutron microscopic reaction cross-section (σ_{rx}), which is a function of the target isotope and incident neutron energy (E_n). The microscopic cross-section multiplied by the atomic number density, N, provides macroscopic cross-section (Σ_{rx}), a measure of the interaction probability in bulk material.

Neutrons can be categorized into energy regimes such as thermal, epithermal, and fast, although these regions are relative and vary according to different fields of nuclear sciences or particle physics. A thermal neutron is below 0.025 eV, which is average neutron energy, (E_n), in thermal equilibrium with a 290 K temperature distribution [26]. Epithermal neutrons are between 0.025 eV and 1 MeV, and fast neutrons are above 1 MeV. In this context of presenting fission product distributions as a function of energy, fast neutrons are a Watt spectrum at 500 keV, and high energy neutrons are 14 MeV.

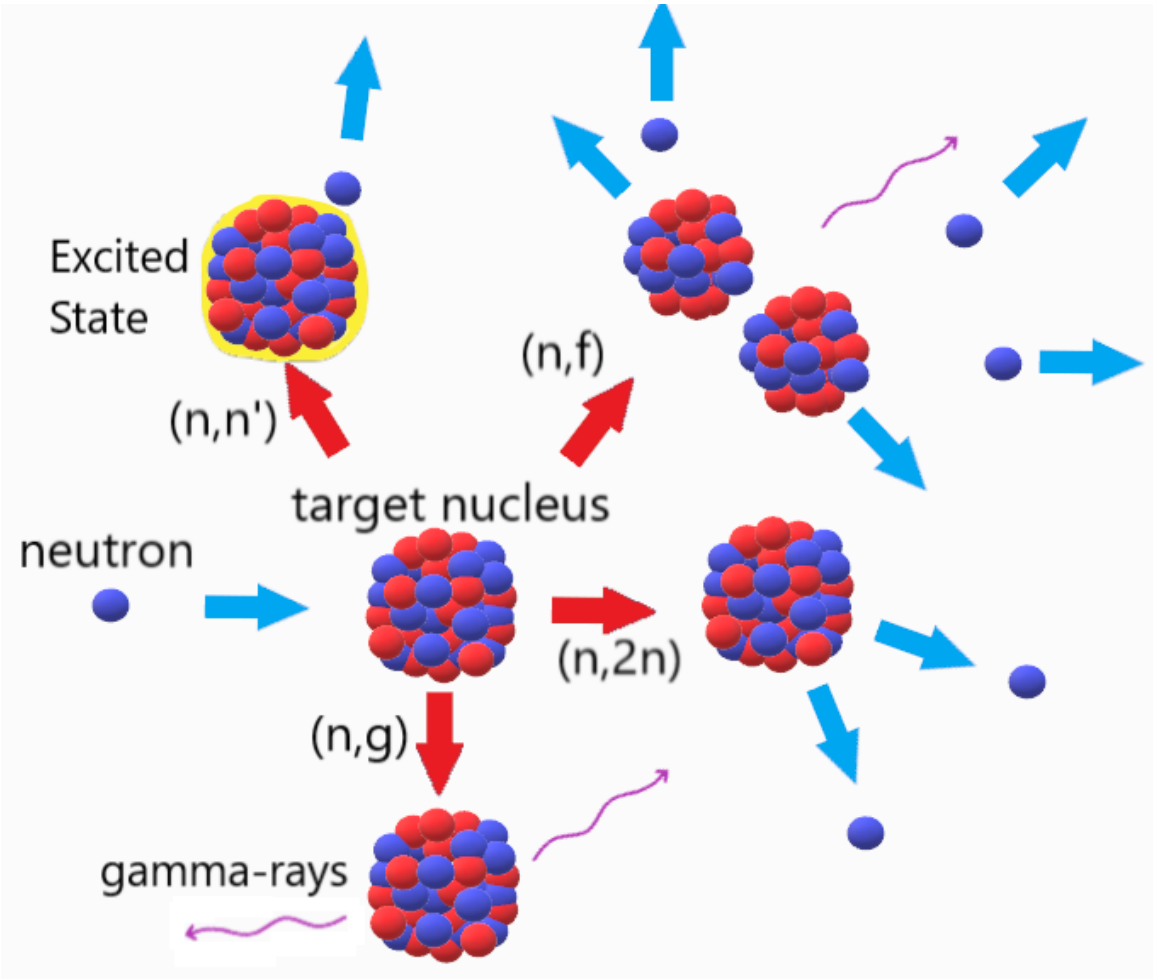

Figure 2. Diagram of selected neutron reactions important to various aspects of this work [25].

2.1.1 n,n

Elastic scattering (n,n) is an extremely important reaction for lowering the average energy of the neutron population by downscattering [27]. An elastic collision does not place the target nucleus in an excited state, which allows for the simplified use of conservation of energy and momentum to describe the interaction. A selected group of elastic scattering cross-sections relevant to the application in an ETA are shown in Figure 3.

The maximum energy lost in a neutron elastic collision with an isotope is a function of the target isotope atomic mass (M). Elastic scatters off higher mass isotopes

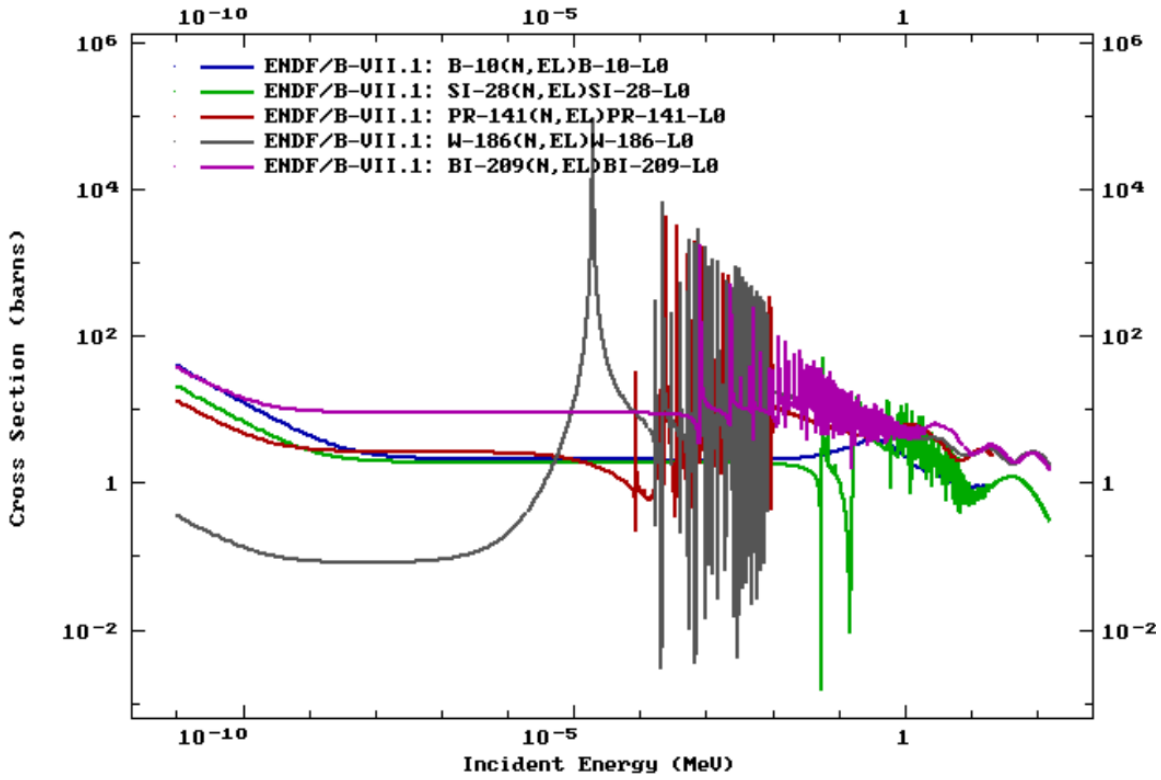

Figure 3. Comparison of various elastic scattering cross-sections for materials in the current ETA [28].

produce a smaller energy loss per collision compared to interactions with low atomic mass nuclei. Elastic scattering can transfer nearly all of a neutron's kinetic energy with a collision on hydrogen, while scattering off bismuth will produce very little energy loss. The maximum energy transfer (Q) to the target nucleus per collision is given by:

$$Q_{max} = \frac{4ME_n}{(M+1)^2} \tag{1}$$

2.1.2 n,n'

Inelastic scattering is similar to the reaction dynamics of elastic scattering; however, the target nucleus is placed in an energetically excited state [27]. These excited states are governed by quantum mechanics and are unique to particular isotopes.

Nuclear excited states akin to the electronic shell structure of atoms. Hydrogen for example can have infinite electron shells with decreasing shell energy differential up to the ionization energy of the electron. An incident photon can populate the electron into an excited states, but nuclear states have a limited number of discrete levels. Two nuclei can form a quasi-continuous spectrum during a compound reaction which gives rise to resonances [29]. These resonances have a certain energy width created by states having a energy widths larger than the energy spacing of the states.

Inelastic scattering is a threshold reaction, meaning an incident neutron must have a minimum amount of energy to enable the reaction channel. Additionally, neutrons generally lose more energy per collision if the interaction is inelastic on high Z isotopes. The energy that would normally be conserved in the collision is reduced in the conservation equations. Examples of inelastic scattering cross-sections are shown in Figure 4. Isotopes from $A = 12$ to 209 are shown to identify the trend of increasing mass number.

Inelastic scattering is one of the lowest threshold energy neutron reactions. As shown in Figure 4, there is no general functional form of the reaction by isotope. Al-27, a lighter isotope, is between W-184 and Pb-208. These cross-sections indicate the energy levels of the nuclei itself. Threshold reactions are also of interest to determining the neutron spectrum for identifying the reaction rate above the threshold energy.

The excited state nucleus can de-excite via gamma emission or other channels if energetically favorable. The excited nucleus usually decays in a short time relative to isomeric states if the inelastic scatter occurs off of a stable nucleus. Isomers are not stable; however, these metastable states can have half-lives on the order of hours or much longer [29]. These isomeric states have applications in foil activation experiments, where it may take some time to start measuring the foil activity. An energy level and decay mode diagram of In-116 is shown in Figure 5. Depending on

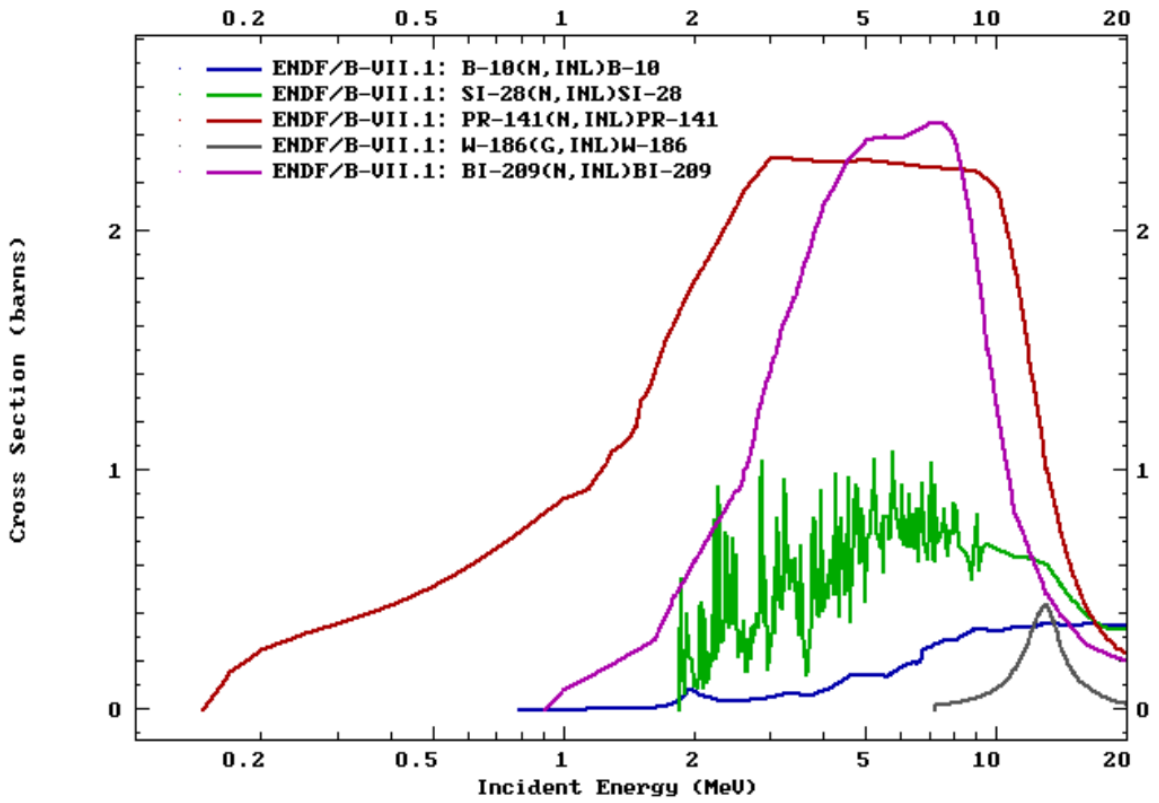

Figure 4. Comparison of various inelastic scattering cross-sections for materials in the current ETA [28]

the selection rules, certain energy level transitions are available for a given neutron interaction [30].

2.1.3 n,xn

A neutron can interact with a nucleus and eject additional particles, such as neutrons or protons. (n,xn) reactions such as (n,2n) and (n,3n) require a threshold energy to separate the neutron from the original nucleus, appropriately called the neutron separation energy. Neutron separation energies are on the order of a few MeV to tens of MeV [29, 31]. Increasing the neutron energy allows for the evaporation of more neutrons from the nucleus.

The (n,xn) mechanism can occur as a direct reaction, where the incident proton

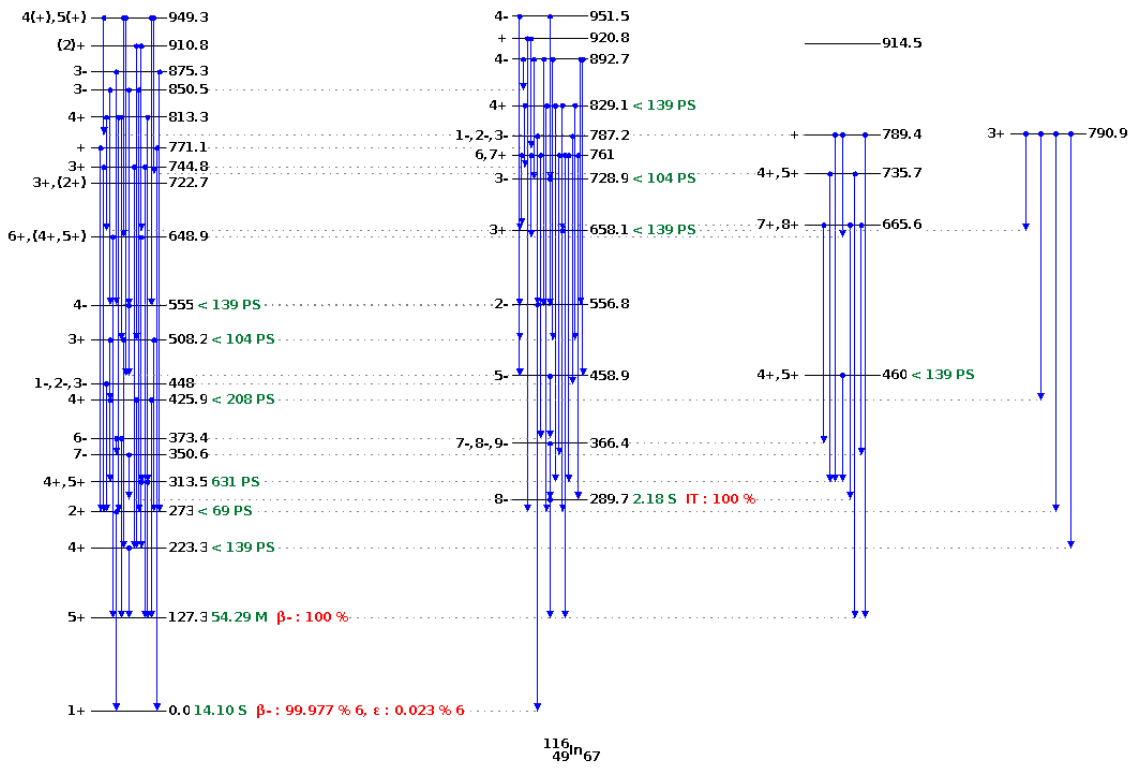

Figure 5. In-116 energy level and decay mode diagram truncated at 970.4 keV. The metastable state at 127 keV with spin parity $J^{\pi} = 5^{+}$ is important for foil activation experiments for the epithermal region. Plots produced using the Online Service retrieval code package written by C. L. Dunford, National Nuclear Data Center, Brookhaven National Laboratory.

interacts with only a few particles in the nucleus. Additionally, the neutron can interact with the entire nuclei and be absorbed in a resonance or compound reaction, later ejecting the particles [27]. There is a large variance based on the internal nuclear structure. Example (n,2n) reactions are shown in Figure 6. The cross-section threshold is generally lower for higher atomic mass isotopes which are not as tightly bound to the neutron.

In the context of spectral shaping, (n,xn) reactions are significant for two reasons. First, the interaction increases the total neutron population which is beneficial for increasing the number of neutrons on the samples. Second, the neutron energy post-reaction is lower because the reaction required to overcome the potential barrier and

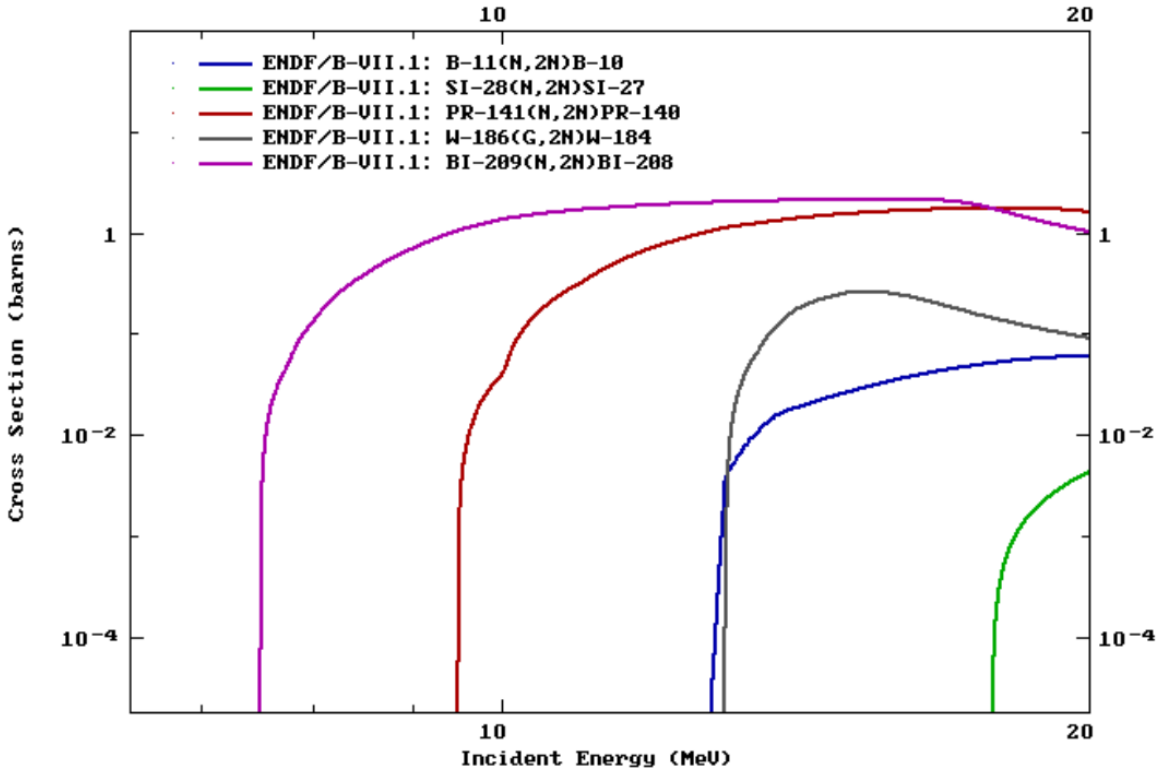

Figure 6. Comparison of various (n,2n) cross-sections for materials in the current ETA [28]

losses through gamma emission. The lowered neutron energy is beneficial again for building up lower energy portions compared to the source term. Additionally, this reaction mechanism has applications in foil activation experiments.

2.1.4 n,γ

Radiative capture, abeled (n,g) and (n,γ) in literature, is a reaction mechanism most prominent at low energies where an incident neutron is absorbed into the nucleus and a gamma-ray is emitted [29]. At low energies (below approximatley 1 keV, isotope dependent) the absorption cross-section follows the "1/v" law, so the probability increases with the inverse of the square of the incident neutron energy [27]. Figure 7 provides examples of selected (n,γ) cross-sections.

Radiative capture is an important absorption reaction mechanism in a few ways.

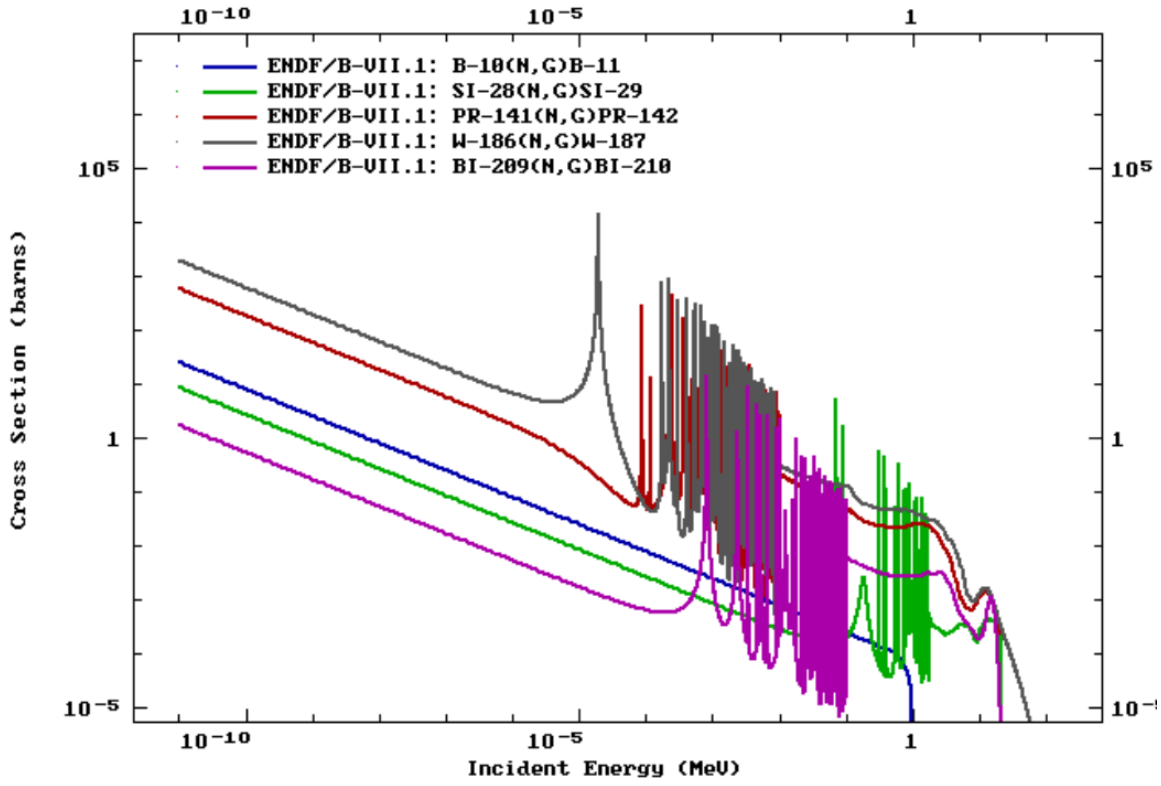

Figure 7. Comparison of various (n,γ) cross-sections [28] for materials in the current ETA

(nγ) reactions are of interest to foil activation experiments, specifically for determining the thermal spectrum. The resonance structure in the epithermal region can also be used to generate a unique response. Radiative capture is generally undesirable for spectral shaping, acting as a poison for the neutron economy. Fortunately, the NIF source, at 14 MeV, is not largely impacted until the neutrons have been moderated, but the (n, γ) reaction can be used to absorb an excess of thermal neutrons [5].

2.2 Nuclear Fission

2.2.1 Fission Theory

Nuclear fission reactions encompass the breakup of an unstable nucleus into two or more fission fragments. Fission releases a large amount of energy (approximately

200 MeV), which is distributed as kinetic energy in the fission fragments, neutrons, gamma-rays, and delayed decay energy. The amount of energy liberated is dependent on the reaction products, so an average number is usually given. The delayed portion is associated with the decay of the unstable fission fragments, which includes energy in the form of beta particles, additional gamma-rays, anti-neutrinos, and neutrons. A schematic of the fission process is shown in Figure 8.

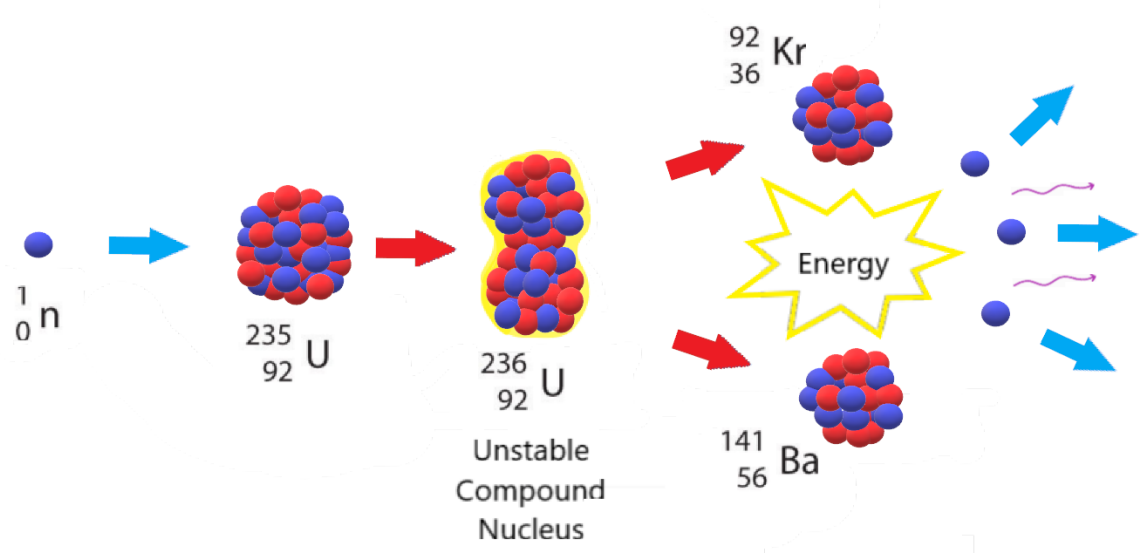

Figure 8. Schematic overview of ^{235}U neutron induced fission.

Fission occurs most often in high atomic mass nuclei, such as ^{235}U, ^{238}U, or ^{239}Pu; however, any isotope can be fissioned at large enough incident energies. The fissioned isotope separates into two or occasionally three nuclei [6]. Fissionable isotopes, for example U-238, Pu-240, Pu-242, have a significant fission barrier, depressed fission cross-sections at low energy, and are incapable of sustaining a nuclear chain reaction. Fissile isotopes like U-235 and Pu-239 are capable of sustaining a nuclear chain reaction and have cross-sections with similar characteristics to the radiative capture cross-section.

The unstable compound nucleus can be modeled at high neutron energies, well above the fission barrier, as an incompressible liquid drop [29,32]. The deformation of

the nucleus causes increased surface energies, which are balanced with the Coulomb (charge repulsion), volume contribution, and shell pairing effects. The perturbation creates an increase to the surface energy and decrease of the Coulomb repulsion because the charge is spread out [33]. During the fission process, the evolving compound nucleus can emit pre-fission neutrons, known as multi-chance fission [33]. First-chance fission is the emission of no neutrons, second-chance fission is the emission of one neutron, and so on; larger neutron energies are correlated with higher order chance fission. The average fission process releases 2-3 neutrons, and the average increases with incident neutron energy. The mean number of neutrons released per fission event is the neutron multiplicity.

Immediately following the fission event, the fission fragments are at a highly excited state. Fission fragments are generally very neutron rich compared to the valley of stability. The excited fragments emit photons to de-excite and may have enough energy to evaporate more neutrons [33]. The prompt fission product yield is the distribution of products post neutron evaporation from the fission fragments.

2.2.2 Fission Products

The fission product distribution from thermally induced fission tends to be centered around isotopes with closed nuclear shells. These isotopes are have a "magic number" of protons and neutrons, similar to the filled electron structure of the noble gases. The fission fragment distribution of thermal neutrons incident on ^{235}U is shown in Figure 9.

Stable nuclei have approximately half as many protons to the total nucleons (neutrons and protons) [29]. Larger nuclei require more neutrons to mitigate Coulomb repulsion. As noted, most of the decay processes following fission are beta emitters, which occurs because the products are rich in neutrons. Figure 10 shows the primary

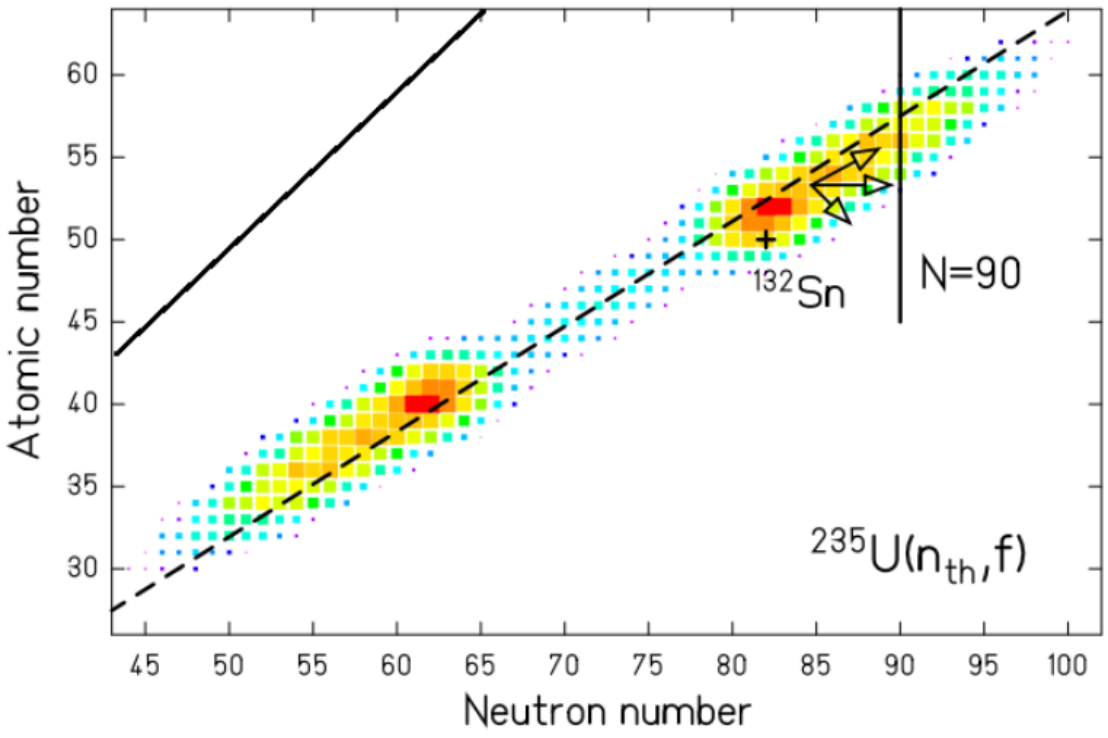

Figure 9. GEF calculated thermal fission product distribution prior to prompt neutron emission. The dashed line is the neutron to proton ratio of U-235 and the solid line is a neutron to proton ratio of 1 [34].

decay modes of isotopes as they decay to the valley of stability. In the region of fission products, the primary competing decay mode is neutron emission, resulting in mass chain feeding and loss after the initial fission process.

Fission yields can be described by the independent, cumulative, and chain yields [35]. The independent yield,Y_{ind}, for thermal ^{235}U fission is shown in Figure 11 which is the fission products directly after the fission event before decay [35]. The fractional independent yield, $f(A, Z)$, defines the yield of a particular isotope. The sum yield, $Y(A)$, is the is the sum of all fission products for a given mass A. The isomeric yield ratio, $R(A, Z, I)$, is the the production of each isomer, I, for a given independent yield. The independent isomeric yield is defined as [36]

$$Y_{ind}(A, Z, I) = Y(A)f(A, Z)R(A, Z, I). \tag{2}$$

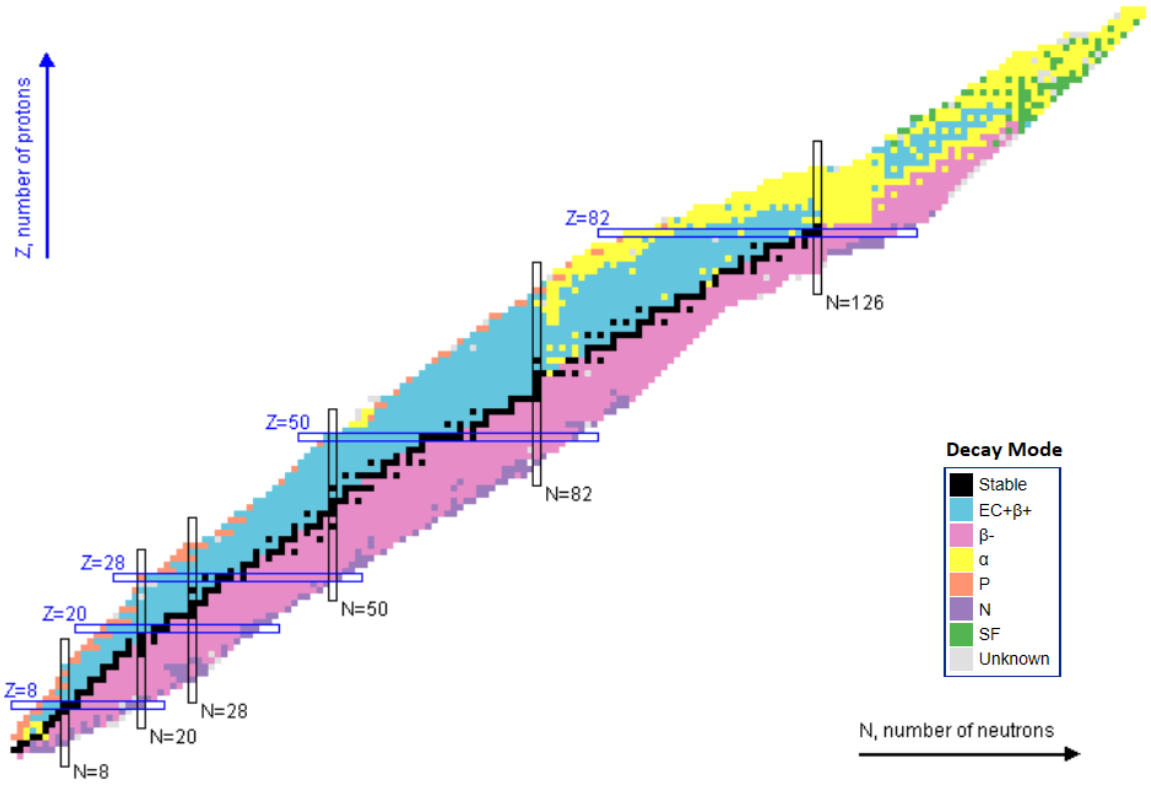

Figure 10. Primary decay modes of isotopes. Plots produced using the Online Service retrieval code package written by C. L. Dunford, National Nuclear Data Center, Brookhaven National Laboratory.

The cumulative yield, $Y_c(A, Z, I)$, represents the production of an isotope produced after all prompt and delayed emissions and decays. The cumulative yield is given as [37]

$$Y_c(A, Z, I) = Y_{ind}(A, Z, I) + \sum_{j=0}^{N} Y_c(A_j, Z_j, I_j)\, b_j \tag{3}$$

where b_j represents the branching from from isotope j into the cumulative yield and N defines the total decay channels into the cumulative yield isotope. The cumulative yields for thermal, fast, and high energy fission of ^{235}U are shown in Figure 12.

The chain yield for a particular mass chain is defined as the sum of the cumulative yields for the final decay to a stable or very long lived isotope in that mass chain [35]. The chain yield leads to the cumulative distribution accounting for branching in and

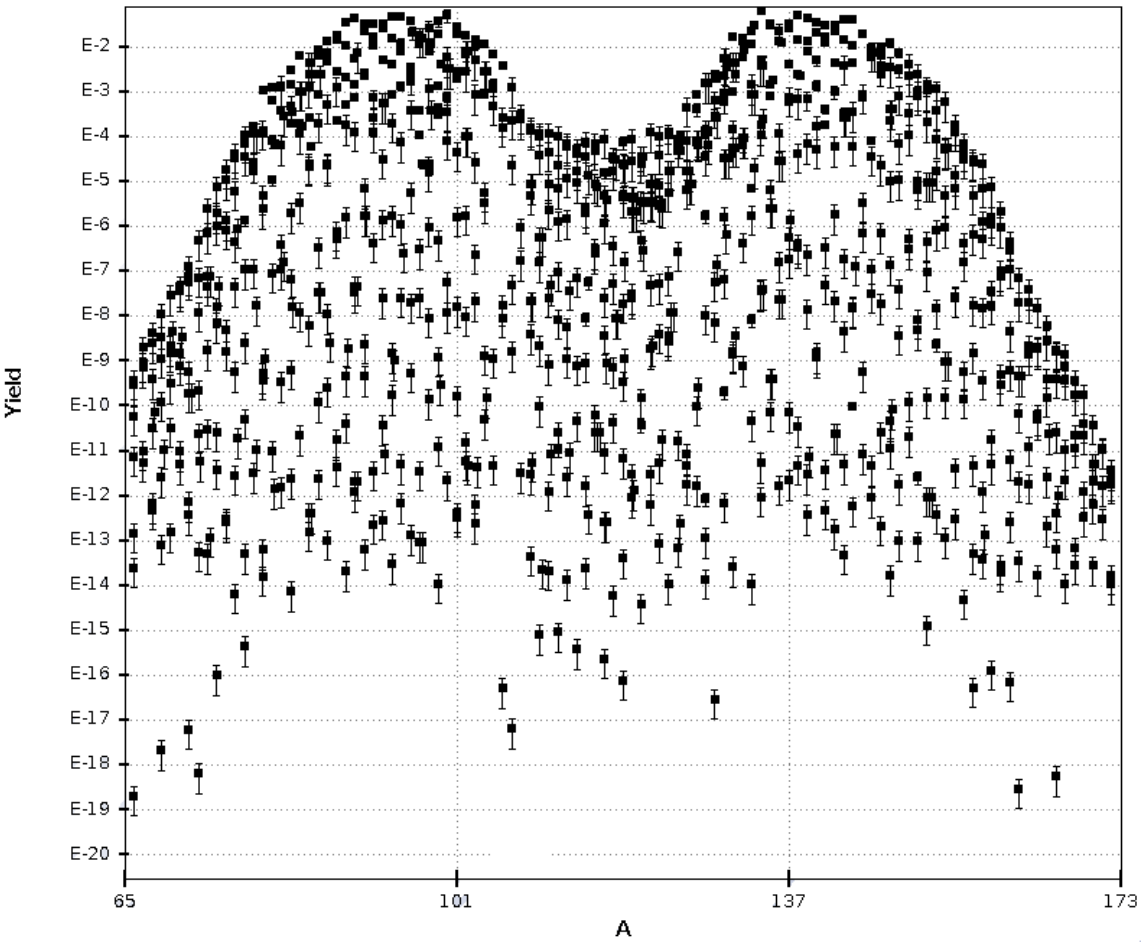

Figure 11. Independent fission product yield of thermal fission of U-235. Plots produced using the Online Service retrieval code package written by C. L. Dunford, National Nuclear Data Center, Brookhaven National Laboratory.

out of a mass chain through neutron emission. An example is shown in Figure 13 for the A = 89 mass chain, where the stable isotope is Y-89 [38]. The neutron deficient decay scheme has not been shown as it has negligible contribution to the fission product decay scheme.

Yields are dependent on the energy of the incident neutron and the fissioning nucleus. As the energy of the neutron is increased, the valley of the fission products is raised as the fission process becomes more symmetric [32]. Additionally, the distribution shifts to larger mass nuclides as the fissioning nucleus mass increases. The uncertainty in the fission product yields varies significantly; the fast fission relative

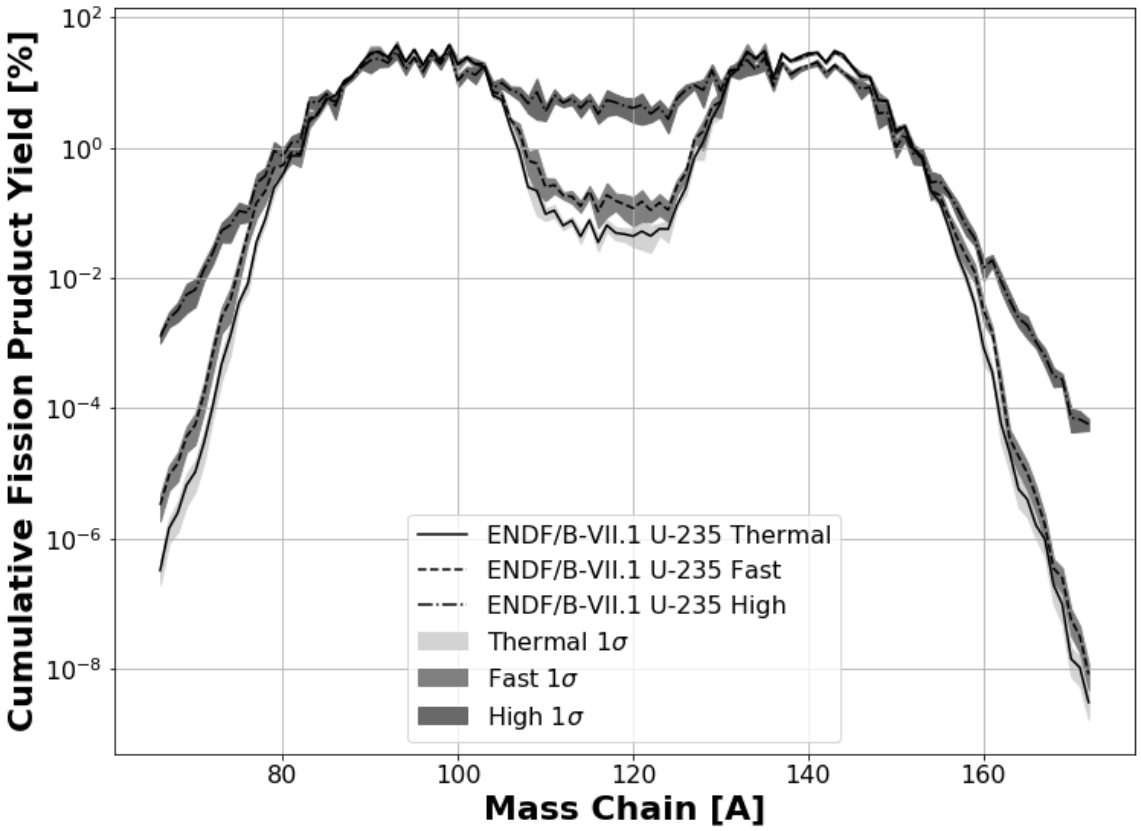

Figure 12. Comparison of energy dependent U-235 cumulative fission product distributions from ENDF/B-VII.1 [28].

uncertainty ranges from 1.6% for mass chain 137 to 64% for mass chain 109.

The radioactive emissions of the final decay can be used to measure the cumulative fission product yield for an isotope. Some mass chains are more well-behaved for measuring the cumulative yield. For example, the $A = 89$ mass chain has many decays that have very short half-lives, up to the precursor stage for the stable isotope.

2.2.3 Nagy Fits for Fission Product Yield

Empirical relations exist to predict the fission product yield as a function of energy given sufficient yield measurement data. Nagy fits the fission product experimental data to an exponential equation

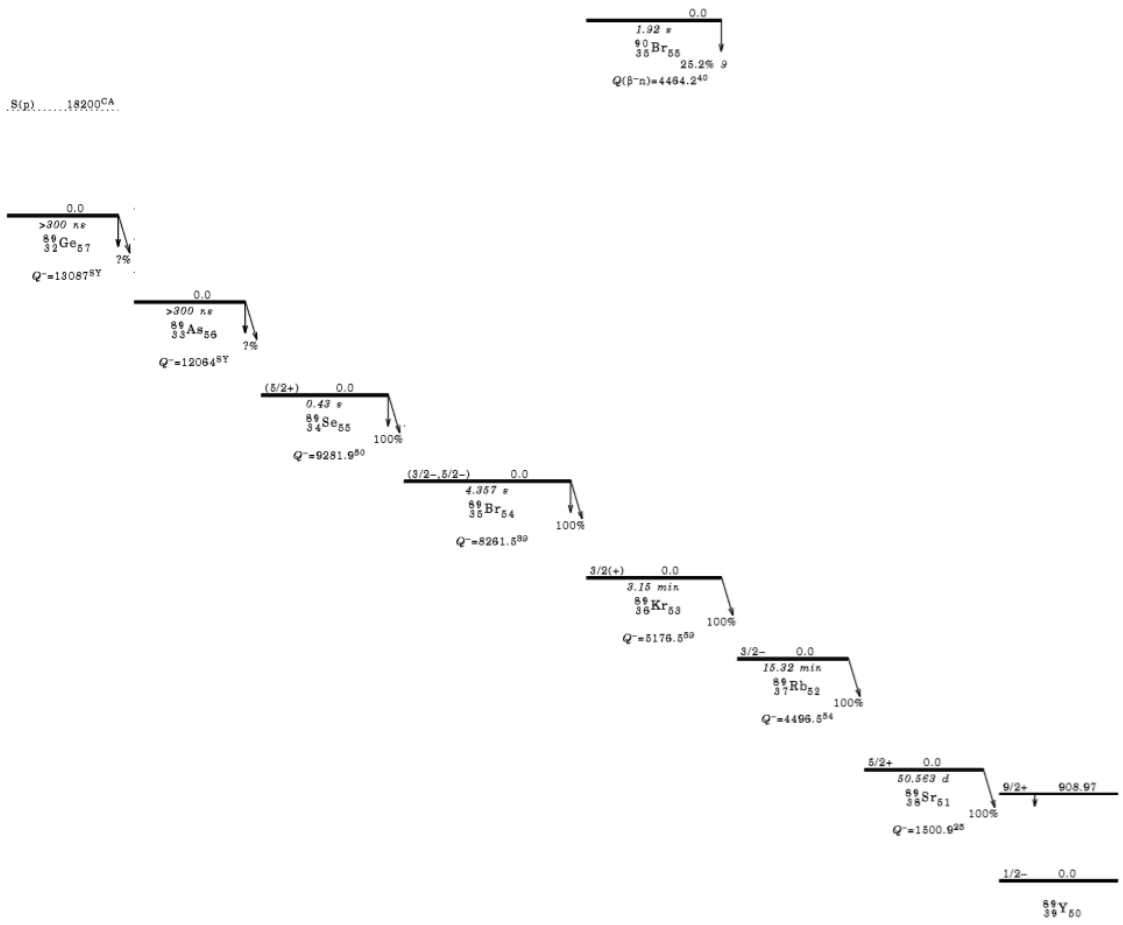

Figure 13. Neutron rich decay scheme for mass chain A=89 [38].

$$Y(E_n) = Y_0 e^{bE_n} \tag{4}$$

The fitting parameters b and Y_0 represent the slope of the function in logarithmic form and thermal fission yield, respectively [23]. The slope is the primary measure of the energy dependency of the fission product yield. The Nagy fit requires modifications for first and second chance fission. First chance fission is dominant from up to 5.5 MeV, and second-chance fission up to 14.1 MeV [23]. The multi-chance fission effects are less likely in asymmetric regions have a larger impact in symmetric fission ($109 \leq A \leq 129$) [5].

It is important to note that data based phenomenological models are not perfect predictors of determining fission products a priori. In particular, recent publications have findings that contradict and cannot be accurately modeled with current theoretical approaches [32]. In general, there are large uncertainties in the predictive power of calculating energy dependent fission product yields.

2.3 Nuclear Data

2.3.1 Nuclear Data Libraries

Nuclear data relevant to neutrons has been collected for the better part of the last century. The experimental nuclear data is collected and published in types of evaluated data files. There are many versions of evaluated nuclear data, which all aim to characterize the relevant physics backed by experimental results. For example, the U.S. nuclear data file is the Evaluated Nuclear Data File (ENDF). Other nations or organizations also have independent evaluations of the available nuclear data. Examples of other nuclear data libraries are the Russian National Library of Nuclear Data (ROSFOND), the European Joint Evaluated Fission and Fusion (JEFF) Nuclear Data Library, and the International Reactor Dosimetry and Fusion File (IRDFF). The various evaluated libraries available have different regions of application. Figure 14 shows the evaluation of Au-197 (n,2n) for various libraries. In some cases, the library evaluation can be drastically different. However, sometimes the libraries are drawing from the same data and models, which can be noted by the overlapping evaluations.

The process from which nuclear data is created varies. ENDF relies on evaluations of data based on experimental quality, statistics, and theoretical basis to fill in the areas where no experimental data exists [39]. ENDF contains the underlying nuclear data (cross-sections, angular distributions, half-lives, ect.) that can be used in simulations. The experimental data that feeds into ENDF is contained in EXchange

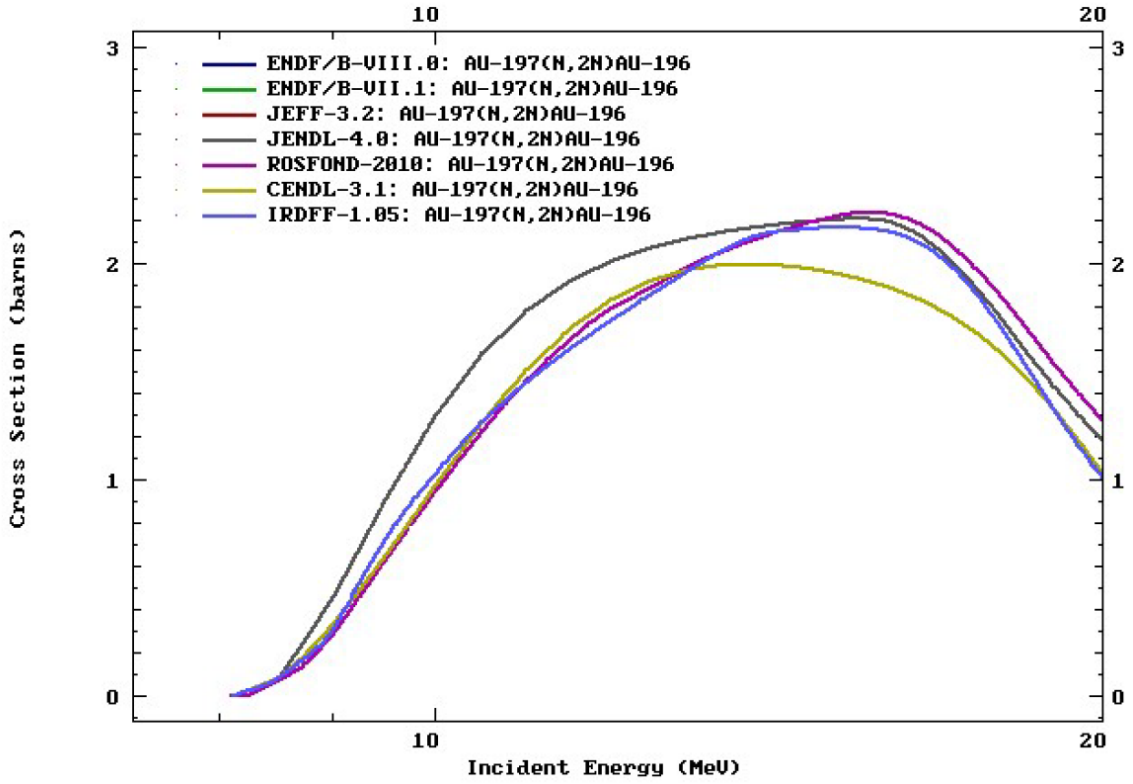

Figure 14. Comparison of various library evaluations of the Au-197 (n,2n) cross-section [28].

FORmat (EXFOR), where the experiment uncertainty, if available, is tracked. A large portion of these libraries are produced with reaction models. Experiments with sub-electron-volt neutron energy resolution are not feasible at the present time, so the nuclear data evaluators need models to fill in the gaps.

Benchmarking the evaluated nuclear data is done primarily through testing of integral results, such as the effective neutron gain to loss ratio (k_{eff}) of a critical assembly [39]. These integral measurements provide a more accessible measurement that can be done with high precision and accuracy, which are used to validate the microscopic nuclear data. Criticality experiments can generally be as precise as a relative error of 0.01% [39]. The use of integral benchmark experiments is important for comparing the net result of the nuclear data; however, there are uncertainties and correlations in the independent reactions that combine to create the integral results.

It is important to note that some experiments, such as gamma spectroscopy, have larger uncertainty by orders of magnitude. An interesting note is that nuclear data values and uncertainty do not always decrease in relative error over time. One example is the increase in uncertainty in the neutrons released per thermal fission of U-235, which increased from 0.311% to 0.385% between ENDF/B-VII.0 to VII.1 [40]. Another example demonstrating the nuclear data problem is that He-6 half-life has changed by approximately 5% with large increases in the relative error over the last 50 years [41]. A sub-second half-life is difficult to measure in experimental facilities. The process of creating nuclear data for application starts with experiment and theory, which is used as an evaluated library. The library is iterated on with validation experiments, applications, studies, and integral benchmarks to increase the base of the nuclear data [39]. The majority of accurate measurements were performed for nuclear reactor studies, which limits accessibility to reliable data for different applications. As a consequence of this, ENDF only contains fission production data at thermal, fast (0.5 MeV), and high energy (14 MeV). There are multiple sources of nuclear data available to help alleviate this issue.

The International Atomic Energy Agency provides (IAEA) provides data for the IRDFF library which contains benchmarked neutron dosimetry reactions [42]. This library is noted because it is used in the PNNL STAYSL code system, which will be discussed later. The IRDFF v.1.05 library contains "state-of-the-art" covariance information and has continuous improvement through testing and integral experiments [43].

The IRDFF library is also convenient in the fact that some of the reactions include feed through from fast decaying excited states to metastable states. An example of this is for the In-116m1, which was shown in Figure 5. The first metastable state at 127 keV (spin parity $J^{\pi} = 5^{+}$) has a half-life of 54 minutes, which makes it a

good candidate reaction for foil activation [44]. The IRDFF v1.05 library contains reaction data which includes the decay of the second metastable state into In-116m1. In-116m2 decays to In-116m1 with a 2 second half-life. Under standard measurement conditions, all of the In-116m2 will decay, thus contributing to the effective activity seen by the first metastable state.

2.3.2 Nuclear Data Covariance

Covariance arises in nuclear related experiments when one process impacts another. Nuclear data covariance is not standard to experimental analysis and many times errors are attributed to model fidelity, measurement, or setup problems when nuclear data covariance might have been the root cause. For example, in many nuclear decay processes, the covariance is unity because the decays happen in a series. However, covariance can occur if there is branching from a radioactive state. Covariance is defined with the expectation values, $< X >$, and mean value (μ)

$$cov(X, Y) = \langle XY \rangle - \mu_X \mu_Y, \tag{5}$$

and the covariance of an observable compared to itself reduces to the variance

$$cov(X, X) = \left\langle X^2 \right\rangle - \langle X \rangle^2 = \sigma_X^2. \tag{6}$$

Nuclear data often stores the correlation matrix using a group structure, as shown in Figure 15, instead of the covariance matrix. The correlation matrix combined with the uncertainty in the nuclear data is equivalent to the covariance matrix. The diagonal of the correlation matrix is one, so the diagonal of the covariance matrix is the variance for the group.

The most straightforward quantity to the covariance matrix is the variance across

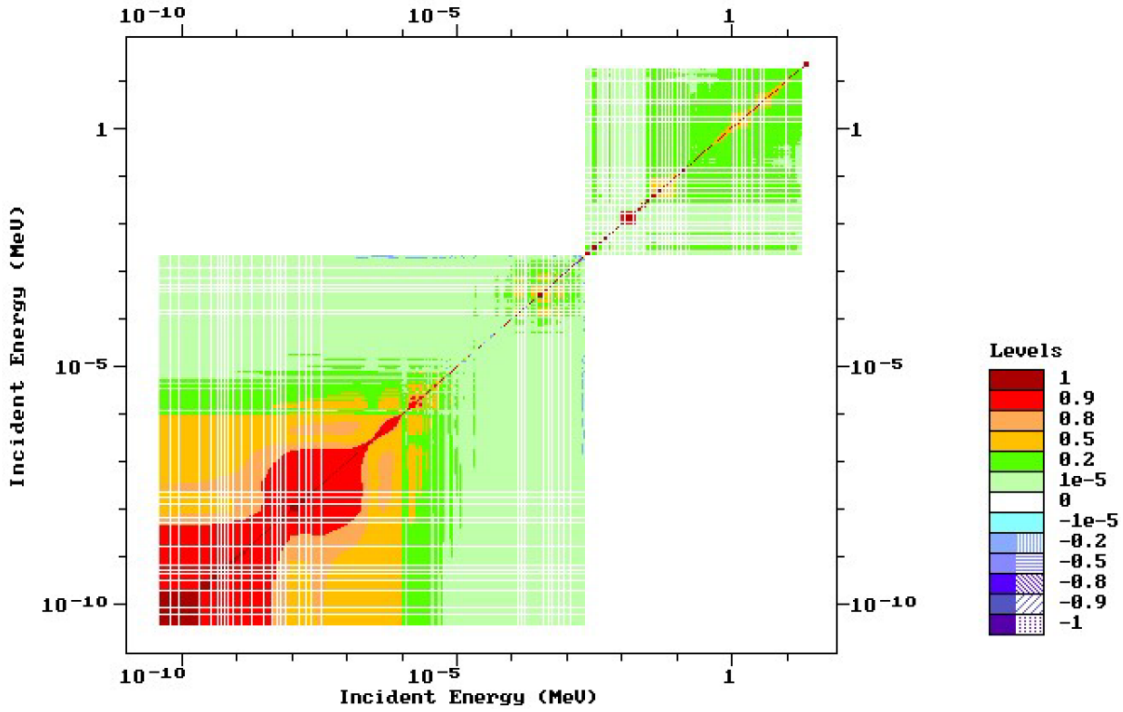

Figure 15. ^{235}U **(n,f) correlation matrix [28].**

the diagonal. Integral experiments are extremely dependent on the underlying reactions that make up the net result. Therefore, there are generally larger variances in the the reactions that are part of the total cross-section. Figure 16 displays the relative uncertainty of the ^{235}U (n,f) cross-section compared to the total. Figure 17 displays the total cross-section of ^{209}Bi to the (n,2n) reaction.

The uncertainty in ^{235}U (n,f) and ^{209}Bi highlight a couple key attributes relevant to nuclear data. First, the component reactions that make up the integral cross-section almost always have a higher relative uncertainty because integral, total cross-section experiments can more accurately be measured through attenuation of a "beam" of neutrons. The underlying reactions are generally more difficult to characterize. The characterization is also dependent on source energy availability, which is not very broad for neutrons. Second, the ^{235}U (n,f) relative uncertainty near 2.2 keV is 133.6%, which implies that the cross-section must go negative to produce the total

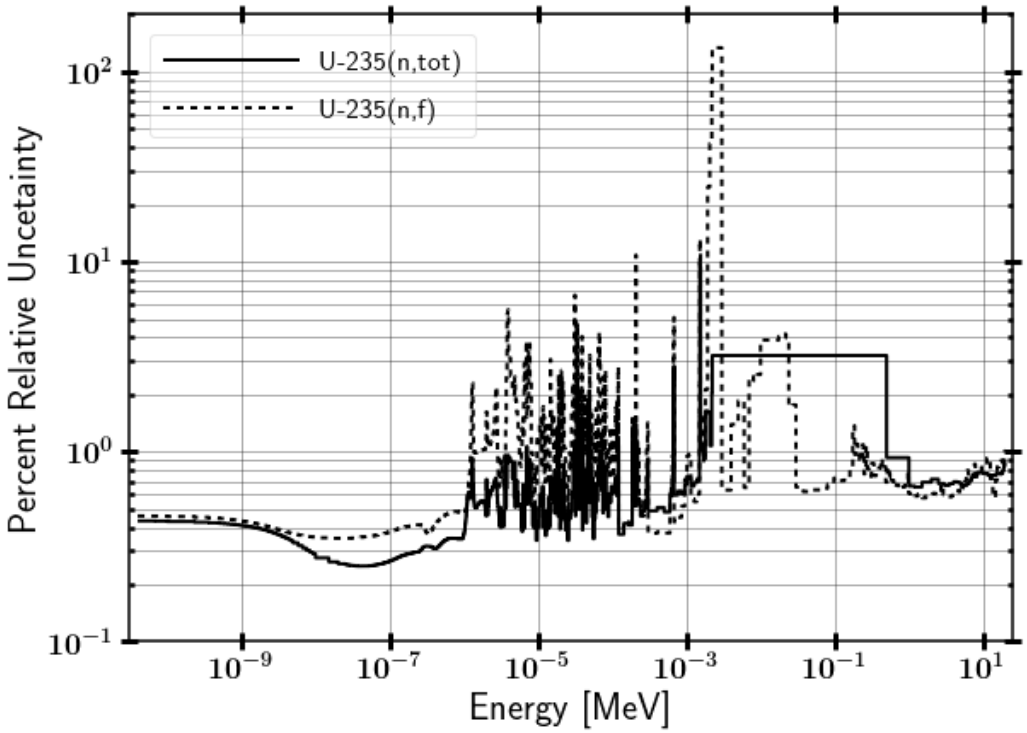

Figure 16. ^{235}U **(n,f) compared to** ^{235}U **(n,tot) cross-seciton uncertainties [28].**

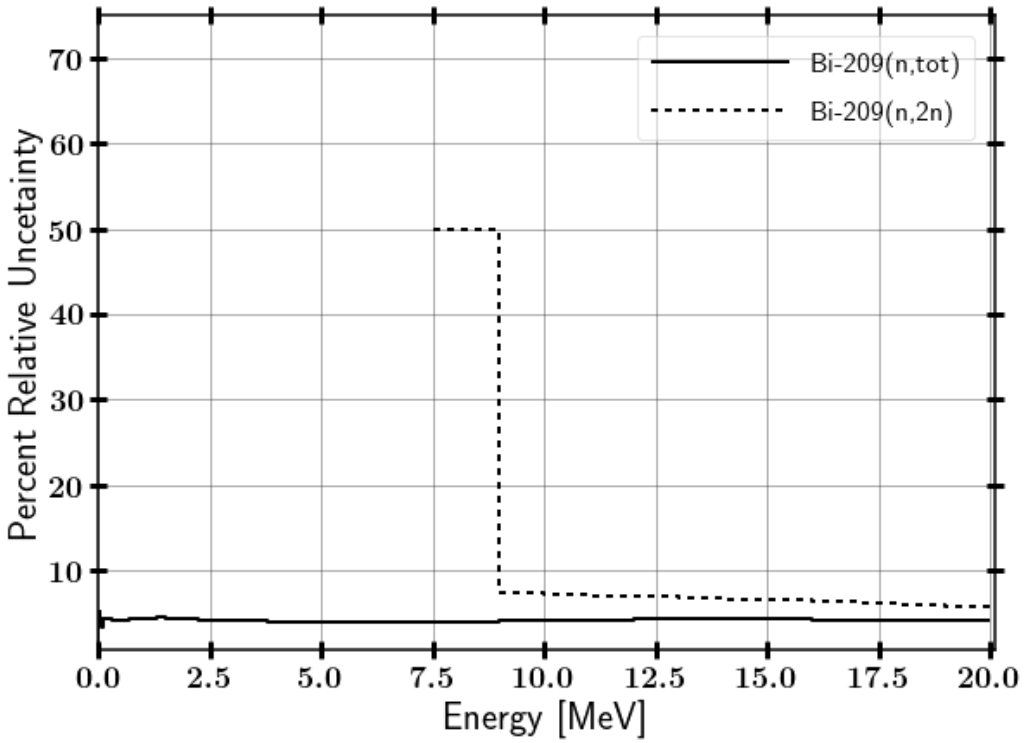

Figure 17. ^{209}Bi **(n,2n) compared to** ^{209}Bi **(n,tot) cross-seciton uncertainties [28].**

total result in some circumstances. This is obviously non-physical; however, it gives scope to the magnitude of uncertainty of the underlying cross-sections over difficult experimental energy ranges. Next, the ^{235}U reactions are more thoroughly studied as compared to ^{209}Bi. Over the the majority of the energy range, ^{235}U is below one percent relative error, largely driven down by thermal nuclear reactor experiments, while ^{209}Bi has a larger error around five percent. Finally, areas where the cross-sections are low have representative larger relative errors, which is presented near the threshold of the ^{209}Bi (n,2n) reaction.

2.4 Monte Carlo Neutron Transport

Monte Carlo (MC) methods for neutron transport leverage pseudo-random sampling, the nuclear data, and material specifications to build up a simulation of the particles [45]. Neutrons are tracked in seven-dimensional space as a function of position, direction, and energy. Neutron interactions are sampled with probability distribution functions (PDFs) for aspects such as path length traveled and interaction type [46].

An objective of a neutron transport calculation is to determine the behavior of particles with in the system. This can be captured with the scalar flux, $\bar{\phi_V}$, defined as

$$\bar{\phi_V} = \frac{1}{V} \int_V dV \int_t dt \int_E dE \, \phi(\vec{r}, E, t), \tag{7}$$

where $\bar{\phi_V}$ is given as a funtion of energy, E, position, $\vec{r}$, and time, t. The scalar flux is averaged over this phase space for some discretization and averaged over a volumetric region. Monte Carlo methods approximate the scalar flux with either track length or collision estimates [46]. The track length estimator is

$$\bar{\phi_V} = \frac{W\,T_l}{V\,N}, \tag{8}$$

where the path length score for the flux based on the length traveled (T_l). The scalar flux is normalized by the particle weight (W), cell volume (V), and number of histories sampled (N).

Statistics often drive the uncertainty in a MC simulation as systematic uncertainties are generally not considered due to computational costs. The "true" mean value, μ, of a response PDF is the expectation value, $E(x)$, which is estimated with a sample mean, $\bar{x}$. The sample mean approaches the real mean as the number of samples, N, goes to infinity.

$$\bar{x} = \frac{1}{N}\sum_{i=1}^{N} x_i \tag{9}$$

The Central Limit Theorem governs the results of Monte Carlo methods and states that for large N, the mean of sampled x_i follows a Normal distribution. The uncertainty is based on the spread of the results.

The variance of the mean, ($S_{\bar{x}}^2$), is based on the sample variance, (S_x^2),

$$S_{\bar{x}}^2 = \frac{S_x^2}{N} \tag{10}$$

where S_x^2 is defined as

$$S_x^2 = \frac{1}{N-1}\sum_{i=1}^{N}(x_i - \bar{x})^2. \tag{11}$$

Therefore, the uncertainty in the results decreases with $\sqrt{N}$. The precision of the result can be improved with more histories, shrinking the spread in x_i. However, the accuracy cannot be improved. Accuracy is impacted by systematic errors. The net

result provides a 1σ confidence bound ($\sim$68% of values lie within 1 standard deviation of the mean).

2.5 Foil Activation

2.5.1 Foil Activation Theory

Foil activation is a method of characterizing an incident neutron flux through unfolding the response of the foils using the energy dependent nuclear reaction channels in the foil. Activation experiments are essential for testing that requires small geometry to fit in the apparatus or in situations where electronics equipment for higher fidelity measuring techniques will be damaged.

The foils intended for activation produce radioactive isotopes during the course of irradiation. The production rate of radioactive isotopes is negated by radioactive decay processes, which place an upper limit on the radioactivity of a foil [30]. The saturated activity (A_∞) is equivalent to the reaction rate (R), which is a function of the energy dependent flux (ϕ), the macroscopic reaction activation cross-section ($\Sigma(E)_{act}$), and the volume of the foil (V). The energy term (E1) is zero in many cases; however, threshold reactions require the incident neutron to be of higher energy to enable the reaction channel. The saturated activity, (A_∞), for a given reaction is given by:

$$A_\infty = R = \int_{E1}^{E2} \phi(E)\Sigma(E)_{act} V \tag{12}$$

A correction needs to be made in cases where the activation is not sufficient to fully saturate the foil. At six half-lives, a foil will have reached approximately 98% of its saturation activity, neglecting spatial and energy self-shielding effects [30]. The activation of the foil for a given irradiation time (t_i) is given as a function of the decay

constant:

$$A_0 = A_\infty(1 - e^{-\lambda t_i}) \tag{13}$$

Experimental measurements also can be corrected to deduce the original activity of the foil, immediately after irradiation. The measured counts, C, is reduced by the background counts, B. A corrects for the radioactive decay for the time between the end of irradiation and the start of counting (t_d). A similar correction factor based on the count time, t_c provides a correction for radioactive decay during counting. Additionally, the detector efficiency for the given gamma-ray energy, ϵ, and relative gamma intensity, I_γ, must be taken into account. The gamma intensity may also include a branching ratio if applicable to the decay mechanism. All corrections included, less self-shielding effects, provide a formulation for converting counts to post-irradiation activity as:

$$A_0 = \frac{\lambda(C - B)e^{\lambda t_d}}{\epsilon(1 - e^{-\lambda t_c})I_\gamma} \tag{14}$$

The formula can be simplified in the limit of irradiation times much less that the half-life of the activation products. In this case, the reaction rate is much larger than the decay from radiation, so the rate of production of the radioisotope is driven only by the reaction rate. The neutron pulse length at the NIF is on the order of shakes, so this approximation can be made for the foil activation. The time integrated flux, or neutron fluence (Φ), can be used to determine the total reactions, (R_{total}), over an irradiation period, given by:

$$R_{total} = \int_{E1}^{E2} \Phi(E)\Sigma(E)_{act} V \, dE \tag{15}$$

2.5.2 Selection of Experimental Foils

The foils selected must meet several requirements depending on the experiment. The method of foil activation has been studied in-depth in the nuclear sciences and engineering community. A list of the various requirements that are of importance for a neutron activation foil experiment with energies in the range of thermal to approximately 20 MeV is summarized [30, 45, 47].

- The reaction neutron cross-section is extremely important for foil activation, and there are a few key parameters that should be considered. First, the magnitude of the cross-section determines the reaction rate of the product nuclides. A large cross-section allows for more activation, and therefore, better results when analyzing the activation foils. Second, the uniqueness of the cross-section shape is used to unfold the incident neutron energy spectrum. An (n,γ) cross-section may peak in a particular region, which is essential to providing information of the neutron flux in that energy region. Alternatively, a threshold reaction, such as an (n,2n), is important for providing information of the flux at higher energies. Third, the selected foils for an experiment should cover the entire energy range of the incident neutron flux.

- The cross-section must be well characterized with low uncertainty over the neutron energy range of interest.

- The decay constant of the product nuclides is important. The half-lives applicable for a particular experiment depend on the time post-irradiation that the foils can be counted. A long lived radioisotope will be available for counting for longer times, but the activity will be reduced due to the lower decay constant. The opposite being true for short half-lives. A half-life on the order of an hour to a few years is in the right direction; however, the half-life must also

be balanced with the production of the radioisotope to understand the entire picture.

- The elemental and chemical purity of the activation foil should be well known. An unknown composition foil will likely cause erroneous results.

- Interfering reaction channels and decay emissions should be avoided. An example of this is natural copper, which has multiple 511 keV emissions from different reaction channels. It is difficult to distinguish these gamma-rays to determine activation in counting. Similar problems arise in multi-isotope materials that have multiple reactions producing the same nuclide. For example, a Cadmium-106 (n,γ) reaction produces the same isotope as a Cadmium-108 (n,2n) reaction.

- The activation foil should be optically thin to not cause perturbations of the neutron flux. An additional benefit of relatively thin foils is that the gamma-ray emissions are not significantly attenuated through self-shielding. The neutron flux should ideally also not be changing substantially over the foil region. In general adding additional foils helps to improve the unfolding results, as long as the entire foil set remains optically thin [48].

- The decay nature of the product nuclide should be a gamma-ray emitter. Gamma-ray detection can provide fine energy resolution to determine activation. The discrete gamma-ray emissions provide a means of determining the source and magnitude of the the foil activation. The energy of the gamma is also of importance. Semiconductor detection methods have a peak intrinsic efficiency near 100 keV with some variance depending on if the semiconductor is p-type or n-type. Beta spectroscopy is also a potential option that will be considered; however, the resolution is not as good as gamma spectroscopy.

2.6 Neutron Energy Spectrum Unfolding

Foil activation experiments are a well established method for determining an incident neutron energy spectrum. The foils are activated under a nearly equivalent neutron flux, which serves to activate the foil samples through nuclear reaction channels, each of the which has a unique response function with respect to the neutron flux. The nuclear data and activities of the foils can be used to unfold the incident neutron energy spectrum. The activated foil production is just the group-wise energy multiplication of the reaction cross-section with the neutron flux.

The activated foil production is just the group-wise energy multiplication of the reaction cross-section with the neutron flux, but solving for the inverse problem for the neutron flux is generally seen as "ill-posed" [48]. In an ideal situation, the number of foils, i, would be selected based on the number of energy groups, j required, and the problem would be formulated as [45, 48]

$$A_i = \sum_{j=1}^{N} \Sigma_i(E_j)\ \Phi(E_j)\ V, \quad i = 1..m \tag{16}$$

In practice, this formulation of the unfolding problem is not used as it often provides nonphysical results. The issue is caused by the varying shapes of reaction cross-sections, which create a poorly constructed matrix and a limit on the number of foils that can be used at a time to prevent changing the neutron flux. There are many methods that aim to provide solutions to the generally degenerate neutron spectrum.

A few examples of studied methods of unfolding matrix inversion, least-squares spectral adjustment, and stochastic algorithms [49]. Direct matrix inversion was previously discussed in the setup of the unfolding problem. Matrix inversion can lead to non-physical results, such as negative fluxes [49]. Stochastic methods rely on random sampling to derive a best-fit or average over a group of reasonably well-

fitting spectra [49]. The least-squares method minimizes the chi-square based on a guess spectrum, activation information, and nuclear data [50]. The least-squares method is also known as spectral adjustment and can incorporate more information, most notably the underlying nuclear data, into the determination of the resultant spectrum [50].

The general formulation of the least-squares method is derived from minimizing the activation results to the nuclear data and input spectrum [50]. The chi-square (χ^2) is given as per degrees of freedom (DOF) as a function of of the uncertainty, activation rates, nuclear data, and measured results. The chi-square formulation of the least-squares approach can be reduced if there is no time dependency of the neutron flux as

$$\frac{\chi^2}{DOF} = \frac{1}{DOF}\sum_{i=1}^{m} \frac{(\sum_{j=1}^{N} \Sigma_i(E_j)\ \Phi(E_j) - \frac{A_i}{V_{Foil}})^2}{\sigma_i^2} \quad . \tag{17}$$

Providing an initial spectrum is generally required for the unfolding methods. The activities produced for the foils is often highly degenerate, where an infinite amount of spectra could provide the same end-point. The initial spectrum allows for the insertion of more physics based results to have an impact on the overall result. For neutron spectra, an initial guess spectrum is often created with a particle transport code or a deterministic solution. Alternatively, an initial spectrum could be selected from published results, where in some applications provide similar results [51].

Several formulations of the χ^2 statistic exist. STAYSL utilizes activity information, A°, a neutron flux and nuclear data matrix, P, and covariance matrices. STAYSL incorporates covariance information, N_P, which is the covariance matrix from the flux and nuclear data. The activity covariance is a matrix given by N_{A°. STAYSL minimizes the χ^2 based on the activity information, $\bar{A}$, and neutron flux and nuclear data parameters, $\bar{P}$. The χ^2 statistic utilzied in STAYSL is given by [50].

$$\chi^2 = \begin{bmatrix} P - \bar{P} \\ A^\circ - \bar{A} \end{bmatrix}^\dagger \bullet \begin{bmatrix} N_P & 0 \\ 0 & N_{A^\circ} \end{bmatrix}^{-1} \bullet \begin{bmatrix} P - \bar{P} \\ A^\circ - \bar{A} \end{bmatrix} \tag{18}$$

3. Methodology

3.1 Computational Setup

Figure 18 displays the research approach methodology with a primary focus on the original ETA. The work performed previously has a completed design for the original ETA. The enhanced fission product ETA and ETA-SPNS will have objective spectra from referenced sources. The computational flow requires a baseline ETA design to use Coeus. Each of the computational steps is explained further below.

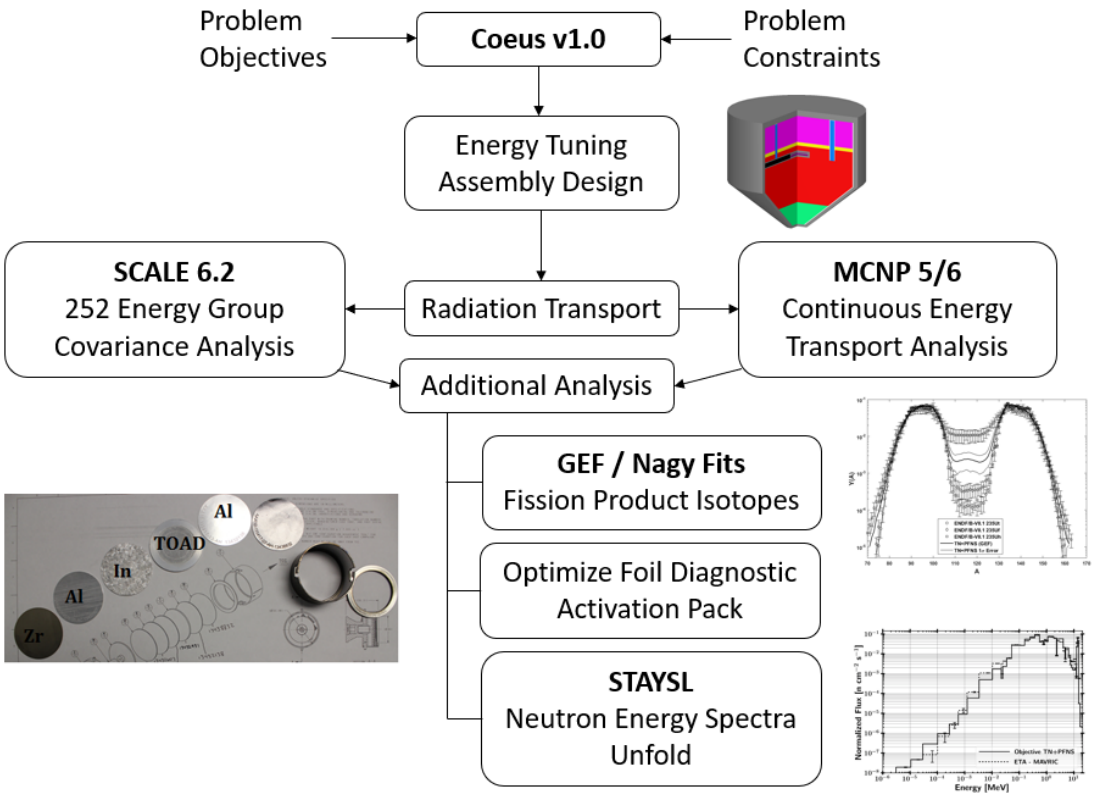

Figure 18. Overview of the major research components for this work and how they are connected.

3.2 Energy Tuning Assembly Design

The spectral shaping problem is defined by the objectives and constraints. For this research, the problem objectives are the three spectra of fission product generation, enhanced fission product generation, and SPNS. The problem constraints are based on the NIF source term and mechanical envelope. The input objectives and constraints are utilized in Coeus to produce a nearly-globally optimum solution for an ETA.

3.2.1 Enhanced Fission Debris Production Objective Spectrum

Still gathering requirements

3.2.2 Short Pulse Neutron Source Objective Spectrum

Still gathering requirements

3.2.3 NIF Constraints

Still gathering requirements

3.2.4 Coeus

Describe any additional considerations in running Coeus here.

3.3 Monte Carlo Transport

Monte Carlo neutron transport will be performed with MCNP and SCALE for the 2019 ETA. The enhanced fission product ETA and ETA-SPNS will only be analyzed in MCNP due to time constraints. The point designs will modeled with MCNP and SCALE version 6.2 to perform neutron radiation transport. MCNP is used for continuous energy solution, while the SCALE's 252 group SAMPLER sequence around MAVRIC is used for group-wise covariance analysis. MAVRIC performs automated

variance reduction techniques along with the traditional Monte Carlo transport calculations. MCNP versions 5 and 6 are both used depending on compatibility with surface source read (SSR) files generated by the NIF and LLNL. Utilizing two different radiation transport models increases the degree of confidence in the results. The radiation transport simulations provide results for the reaction rates for foil activation, neutron energy spectra, and temporal aspect of the neutron flux.

3.3.1 MCNP

The SSR file was used to create sources representing the incident flux from the DT capsule and room return. The SSR file was initially created with the supporting equipment; however, no other experiments were involved. The SSR file contains two disk sources at the front and back of ETA and a cylindrical source on the sides of ETA. The surface fluxes were extracted using surface tallies in MCNP5, because the initial surface writing was performed with MCNP5. The geometry of the surface writing is shown in Figure 19.

The normalized probability distribution functions for the source locations are shown in Figure 20. The surface facing the source was approximated as a point source with the 14.03 MeV neutrons defining 1 source particle with a strength of 1.0063 source particles. The side cylindrical sources was approximated as four surrounding line sources at the same height which emitted at a solid angle to encapsulate the ETA. Ideally, the cylindrical source could be mapped over with a cylindrical source; however, the reference directions for emission in SCALE are in Cartesian coordination. The strength of the cylindrical source was $6.94 * 10^{-4}$ source particles split into the four line sources. The back disk source was modeled as a uniformly emitting disk source with a source strength of $9.44 * 10^{-4}$ source particles. The down-scattered neutrons are the "room return", which is a orders of magnitude below the actual

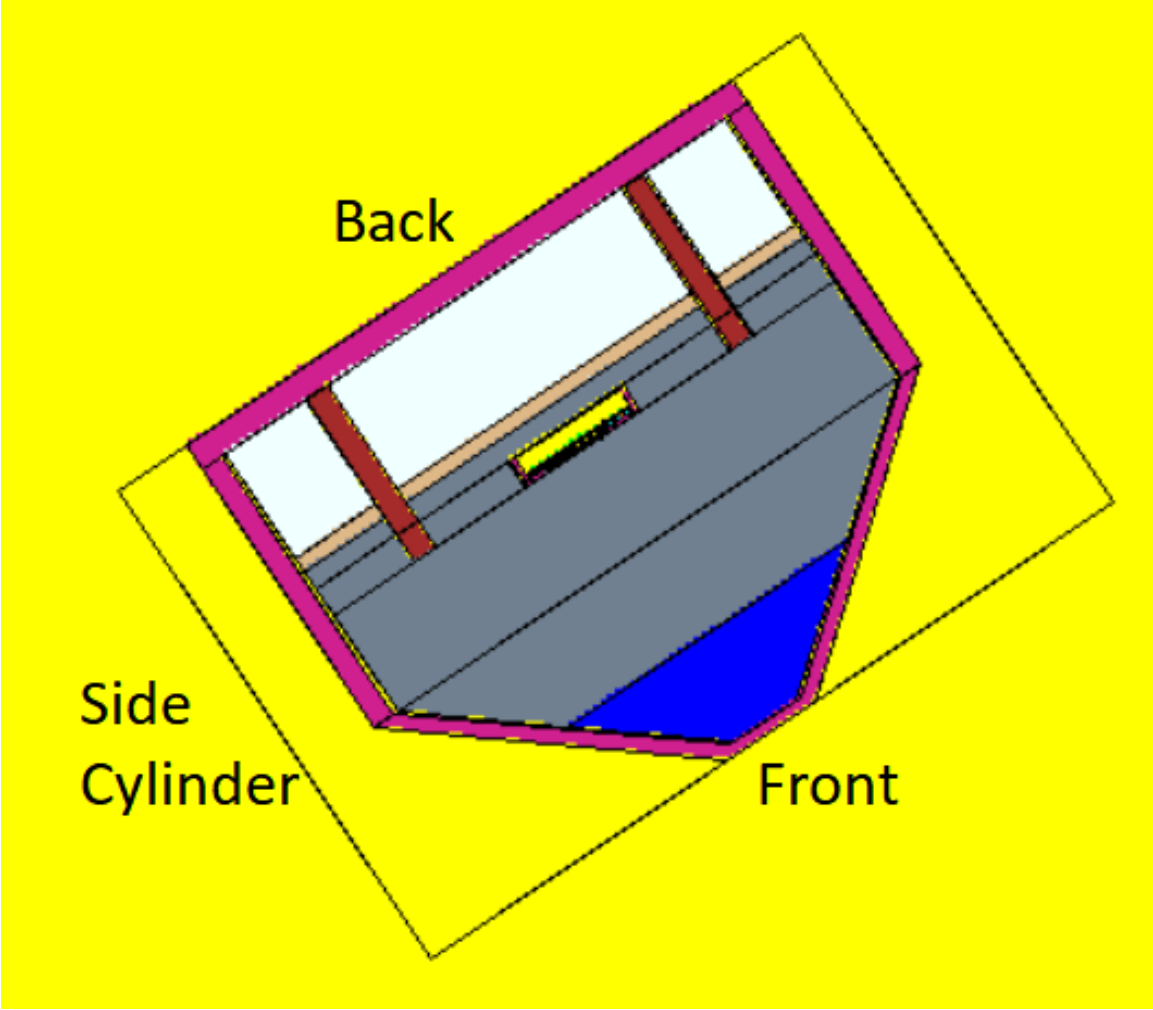

Figure 19. Surfaces for NIF source SSR file.

source neutrons. Still, it is important to capture the impact of the room return, because the neutron cross-sections are in general larger at lower energy.

The results from MCNP are used to benchmark a continuous energy solution in MAVRIC. Although it is not feasible to perfectly replicate the source distribution because there are many scattering angles crossing a surface in different directions, it is possible to get adequately close for the purpose of quantifying the impact of nuclear data covariance. The benchmarking of the mapping of MCNP to SCALE is performed by comparing the reactions in the foil pack. Two key aspects are important. First, the magnitude of the reactions nearly equivalent to about 1%. Second, there

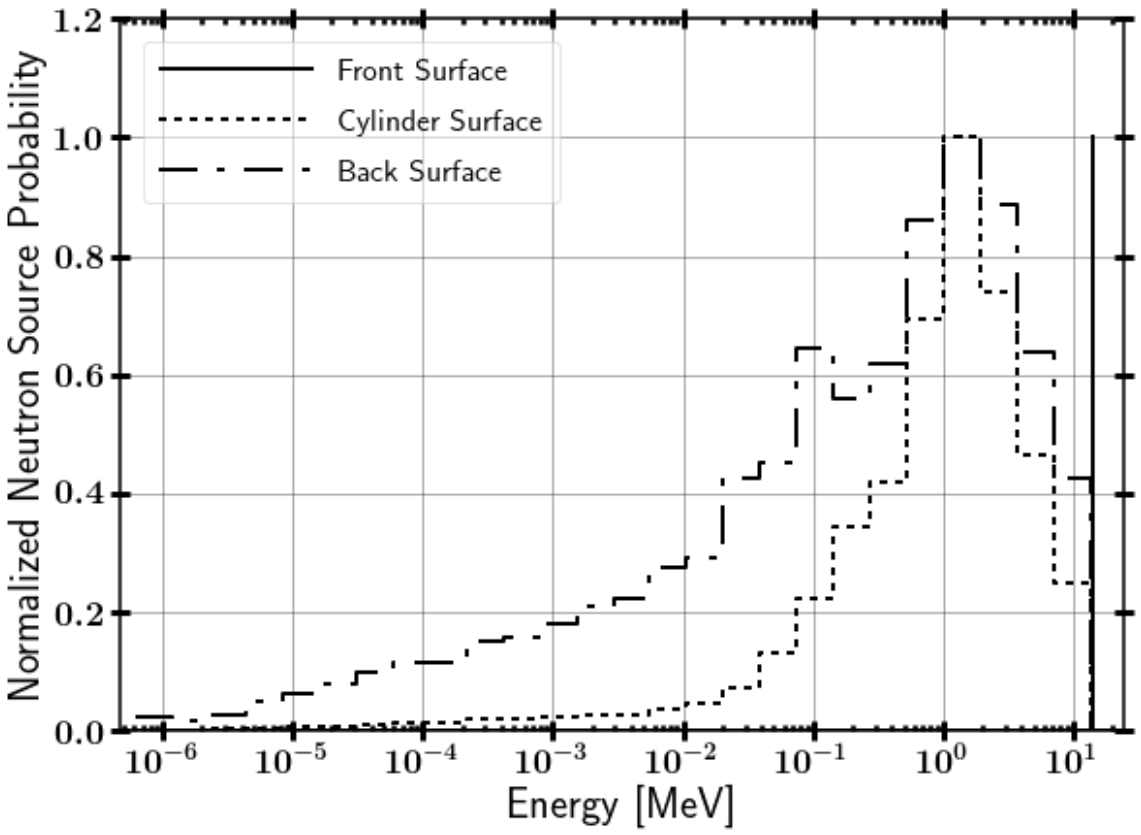

Figure 20. Surfaces source probability distribution functions mapped to SCALE.

is no pattern to the differences between SCALE and MCNP. Examples of important aspects that were looked for are that all the threshold or thermal reactions are not weighted heavily toward SCALE or MCNP.

3.3.2 SCALE SAMPLER Module

SAMPLER is a SCALE module that enables analysis of nuclear data covariance. The unperturbed nuclear data is executed along with a user-defined number of samples. The samples have perturbed nuclear data based on the covariance. SAMPLER is distributed with 252 and 56 energy group structure libraries that have been created with evaluated data and approximated data. The covariance libraries are largely developed from ENDF/B-VII.1; however, additional information has been included from

ENDF/B-VI, ENDF/B-VII.2 (proposed at the time), JENDL-4.0, and collaborative research between Brookhaven National Laboratory, Los Alamos National Laboratory, and Oak Ridge National Laboratory. Finally, the nuclear data covariance libraries include information completed in the Working Party on International Nuclear Data Evaluation Cooperation Subgroup-26 [52].

SAMPLER requires on the order of hundreds samples to provide convergence of the responses [52]. The longer computational nature of SAMPLER runs is a constraint on the computational time available given the number of cores that can be used. Additionally, there are some issues with the SAMPLER sequence that have been addressed to ORNL, but may have an impact on the results. First, particles are sometimes "lost" in the simulation when traveling near parallel to a plane. It was determined that the lost particle effect was primarily due to the neutrons hitting a weight window boundary that is coincident with a plane in model. Second, some samples fail on execution when conducted on parallel. It is expected that the next large update to SCALE will fix these issues.

3.3.3 Comparison of Monte Carlo Neutron Transport Results

The results from a Monte Carlo simulation often produce slightly different results when produced with different codes.The outputs are generally in more agreement for criticality continuations of critical assemblies and nuclear reactor analysis. It is important to gauge the impact to see how much variance is expected. Some of the differences are within the structure of the code itself, statistical error, different starting seeds, while others are based on the nuclear data that may be altered, or ultimately user error in setting up the geometry or source implementation.

Criticality in particular is a well-understood nuclear engineering problem that the nuclear data libraries are validated against. A study conducted on a high temperature

pebble-bed reactor compared SCALE's version 6 CSAS6 code for criticality calculations to MCNP5's kcode [53]. The results showed a difference for calculating k_eff to be on the order of a few hundred percent mile $(10^5 * (k_eff - 1)/k)$. This variance can easily be handled for reactor operations; however, this highlights that even well understood problems do have differences based on operating code. A similar study of a pebble bed reactor with varied geometry determined that the difference in MCNP to SCALE was near half a percent error [54].

A different study was conducted to determine the average gamma-ray doese outside of a spent nuclear fuel cask [55]. The difference in dose rates between identically modeled SCALE and MCNP simulations varied as much as 27%. Again, this shows that the less benchmarked studies can have larger errors which may be caused by user error.

3.3.4 Statistical Bootstrapping of SAMPLER Results

SAMPLER is rooted in stochastic sampling of the nuclear data covariance data [52]. Each sample in SAMPLER is a perturbed set of nuclear data for the Monte Carlo simulation. It is suggested that a typical number of samples is approximately a few hundred [52]. SCALE is distributed with 1000 pre-built samples for each available group structure.

The results of each of the sampled nuclear data libraries with covariance can be combined using statistical bootstrapping. Bootstrapping is a method to determine uncertainty in a given dataset by using random sampling with replacement. First, a sample generated is randomly selected between 0 and n samples. The 0 sample is the unperturbed nuclear data result, while the 1 through n samples have perturbed nuclear data. Next, the value of the corresponding sample number and the relative uncertainty associated with the response are used to sample a gaussian distribu-

tion. The gaussian distribution individual bootstrap trial value selected based on the sampled value and the uncertainty, given by the relative error. A diagram of the SAMPLER bootstrapping process is shown in Figure 21.

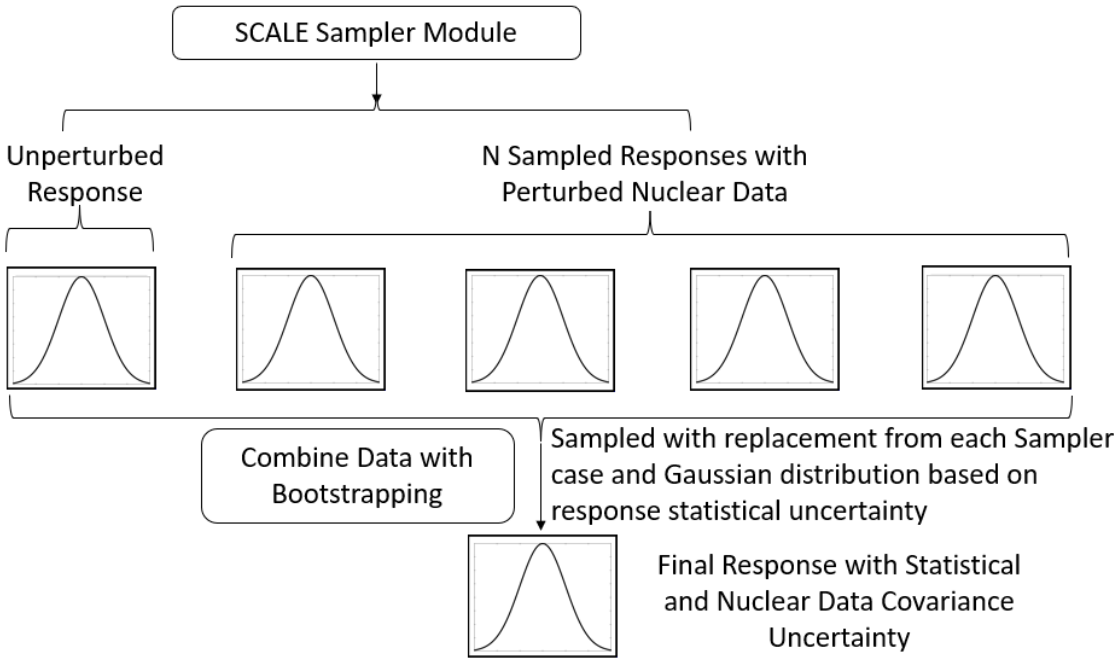

Figure 21. Bootstrapping process utilized to combine SCALE SAMPLER results diagram

Several python functions were built to parse and perform bootstrapping on the SAMPLER outputs. First, the responses are read in, sorted, and stored. The stored data energy group strucutre is collapsed into a smaller group size to reduce uncertainty in the lower energy bins. The results are bootstrapped 20,000 times for each sample used in SAMPLER to provide approximately 0.1% convergence of the bootstrapped relative error. The process of random sampling is conducted with replacement to build up the sampled trials, which are used to find the mean and standard deviation of the bootstrap trial distribution. The bootstrapped values are equivalent to a gaussian distribution if the underlying data is Gaussian in shape. Bootstrapping is useful to use here if a distribution of responses is not perfectly Gaussian, or behaves in an

unexpected manner. The final value and relative uncertainty are used as the final result, which includes nuclear data covariance (a systematic uncertainty) and statistical uncertainty. Other forms of systematic uncertainty will not be fully quantified. For example, the NIF source itself is a potential area of a large systematic uncertainty. The impact of perturbations to the source is explored separately in Section ???.

3.4 Activation Foils

3.4.1 Activation Foils Selection

A foil pack designed to be placed in the ETA experimental cavity will be created to be able to successfully unfold the incident neutron spectra from the activation foils. The activation foils are selected with many important factors. The most notable aspects are the confidence in the nuclear data and energy range that the foils are activated.

A study concluded, based on the energy groups ranging from 0.01 eV to 18 MeV, that Au, As, Cd, In, Ir, Er, Mn, Ni, Se, Sm, W, and Zn are suitable to fully cover the neutron energy spectrum [48]. Key factors for the foils requirements included the cross-section, gamma emission, and half life. The half life was longer than 1 hr to enable off-site measurements, which is of interest for the experiment at the NIF.

The foil pack used in the 2019 experiment will not have enough space to fit all of these foils. A preliminary set containing Au, In, Ni, W and Zn will be tested with the nuclear data activation rates to see if the foil pack is adequate.

3.4.2 Neutron Flux Unfolding with STAYSL

The modeled foil activities are used with the underlying nuclear data to unfold the neutron spectrum using Pacific Northwest National Laboratory (PNNL) STAYSL. STAYSL relies on generalized least-squares spectral adjustment based on the chi-

squared of the measured activities to determine the incident neutron flux [24]. The nuclear data-covariance uncertainty is used as the activation uncertainty in the unfolding, which will provide a higher level of confidence in the spectral agreement. The true activation uncertainty will almost certainly be below that of the nuclear data covariance sampled values.

STAYSL's utilizes data from the IRDFF v1.05 library because of the increased level of benchmarking for dosimetry applications. Therefore, only reactions with data available in IRDFF are considered. Other reactions and foils are of interest; however, the foils included in STAYSL and IRDFF should be suitable.

3.5 Fission Product Generation

GEF is utilized for developing the expected fission product isotopics. GEF is a Monte Carlo and theory based approach that incorporates experimental data to determine fission observables, such as fission products [22].

GEF is applicable over a wide array of fissioning systems including isotopes with a atomic number from 80 to 112 [56]. Potential energy surfaces of the fission barrier of the fissioning system, theory, and adjustments based on empirical parameters have shown good predictive power [34]. The modeled error can often be less than the experimental error. GEF incorporates covariance information and multi-chance fission, amongst many other attributes. Depending on the fissioning system, there are approximately 50 parameters that have been fit to align with experimental results. The inputs to the GEF model are the fissioning nucleus and energy of the incident particle.

Nagy fits will also be used for comparison to GEF. An empirical fit to measured data not included in experiments is beneficial for comparison to GEF.

3.6 Research Approach

Describe why you plan to apply your methodology. For example, prior researchers may have implemented similar methods. On the other hand, if your methods depart from standard practices or improve com- monly used methods, you should state so. Describe how you plan to implement your methodology. For experimental work, you might discuss how you plan to evaluate your equipment and procedures. Computational work should include a discussion of methods that were developed by others, but that you'll implement, as well as the development of code that you plan to write.

3.7 Uncertainty and Error Propagation

The calculated uncertainty in the results is driven by statistical uncertainty from Monte Carlo methods, $1/\sqrt{N}$. In addition to statistical uncertainty, the nuclear data covariance uncertainty provides one form systematic uncertainty.

3.7.1 Error Propagation

Error propagation is important to some aspects of this analysis. One example where error propagation is required is when the 252 group structure from SAMPLER is collapsed. It is important to properly account for and track uncertainty through the entire problem.

The propagation of uncertainty for a function (q) is the square root of the sum of squared uncertainty, (σ_x), of the variables, ($x, y, z, ...$) multiplied by the the partial derivative of the function with respect to that variable [57]. The error propagation formula is given as

$$\sigma_q = \sqrt{(\frac{\partial q}{\partial x}\sigma_x)^2 + (\frac{\partial q}{\partial y}\sigma_y)^2 + (\frac{\partial q}{\partial z}\sigma_z)^2 + ...} \tag{19}$$

3.7.2 Chi-square Statistic and Interpretation

The chi-square statistic, (χ^2), is a useful tool for the interpretation of results to expected results. The reduced χ^2, as used in the foil activation neutron flux unfolding, is [57]

$$\frac{\chi^2}{DOF} = \frac{1}{DOF}\sum_{i=1}^{n}\left(\frac{\textit{observed value - expected value}}{\textit{observed standard deviation}}\right)^2 \tag{20}$$

The degrees of freedom are defined based on the observed data points and parameters computed to fit the equation. The degrees of freedom is the number of measurements in one data set minus one for the case of comparing two data sets.

The expected value for χ^2/DOF is unity if the calculated distribution is described by the expected distribution. χ^2/DOF much greater than one indicate that there is indeed a difference between the expected distribution and the observed. The χ^2/DOF can be used to assess goodness of fit between two distributions.

The p-value can be used to compare the results of the expected distribution to the calculated χ^2/DOF. The p-value is the probability of finding a larger χ^2/DOF, given the calculated result. The test of independence shows the probability of rejecting the null hypothesis, that the two distributions are the same. This probability is governed by the shape of the χ^2 distribution. An example of this is a χ^2 of 16 with 4 degrees of freedom. The p-value from this is 0.003, which implies there is a strong significance of the results not being governed by the expected distribution. The null hypothesis is the rejected. A p-value of 0.05 is generally accepted as statistically significant; however, this can change depending on the field of study. Not rejecting the null hypothesis means the measured results are consistent with the expected; however, the χ^2 test for independence cannot be used to prove the

3.7.3 Systematic Uncertainties

Systematic uncertainties, if known, are propogated exactly the same as error propagation formula. However, the systematic uncertainty is not known in many cases. The aspects of systematic uncertainty for the NIF experiments are discussed here.

Geometric systematic uncertainty based on the positioning of the ETA, DT capsules, or components of ETA has the possibility to introduce systematic uncertainty. The NIF facility has rigid tolerances for positioning systems. It is assumed that the geometric uncertainty of this type is negligible.

A related uncertainty that may arise is the configuration of the NIF chamber. The planned configuration may not be the exact experiment performed, which ultimately requires that the analysis is repeated post-experiment if large perturbations are seen. An example of a change for the experiment might be another experiment in the room. A first order assessment looking at spheres of aluminum and lead simulating other experiments nearby showed that the total number of fissions for 2019 experiment can deviate by a few percent. All material in the chamber can cause backscattering and impact the solution to some degree.

A source of systematic uncertainty is the neutron source itself, which is difficult to characterize completely. A scoping study was performed to analyze the impact of the source on the results. The interpretation of individual results will be presented later; however, it is important to understand to what extent the source may impact the solution. A 14.03 MeV point source is compared to a 10.75 keV plasma temperature Appelbe point source centered at 14.06 MeV, a 14.06 MeV point source, the LLNL full NIF transported MCNP SSR, and the SCALE continuous energy results with the MCNP SSR mapped. The results for the comparison are shown in Figure 22.

The comparison shows a few key details. First, using higher energy source terms (Appelbe or 14.06 MeV) impacts the threshold reactions by as much as 2%. The

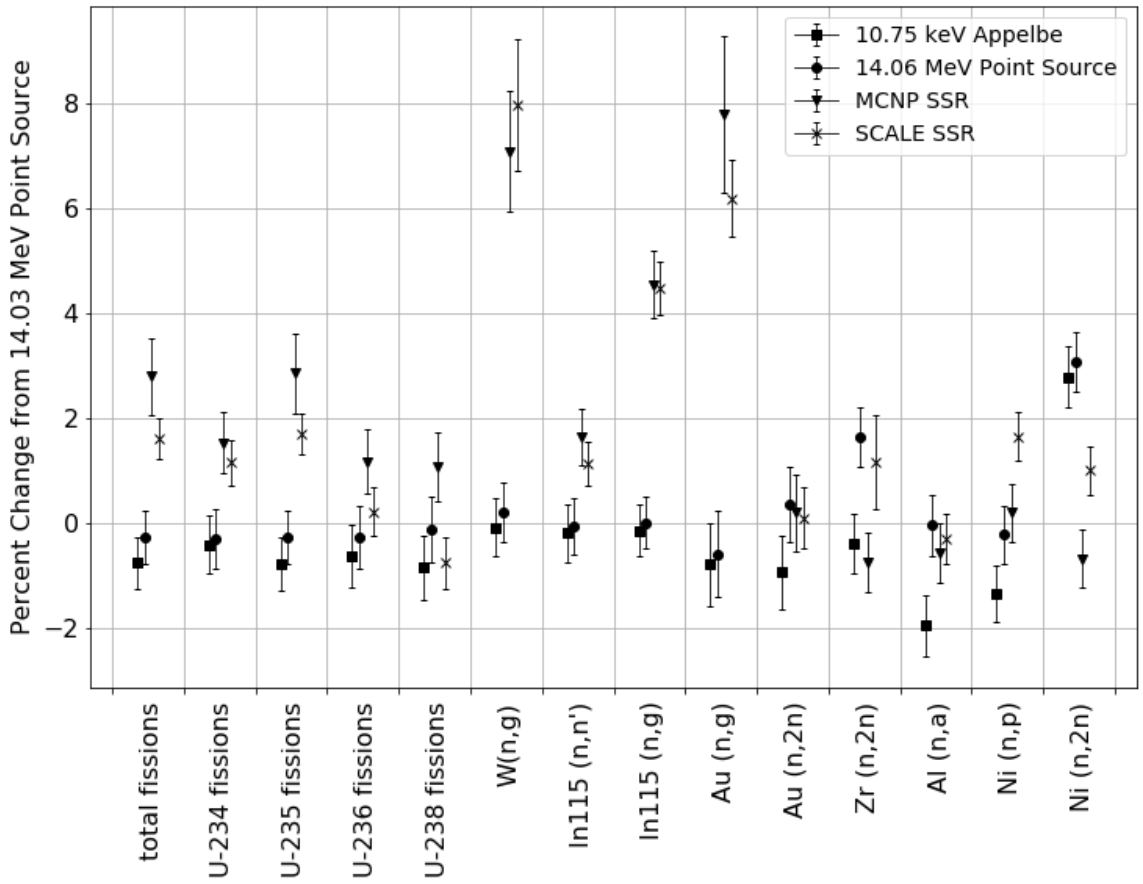

Figure 22. Comparison of results based on NIF source term. The statistical uncertainties of the underlying datasets are all less than 1%

increase based on energy is expected as threshold generally increase with incident energy. Second, the thermal reactions increase substantially by including the room return and scattering back from the DIM. The down-scattered neutrons have lower energy and can contribute more to the total response. Last, the comparison between MCNP and SCALE SSR results is generally consistent. The deviations from the mean are not systematically distributed; for example not all MCNP threshold reactions are larger.

4. Research Schedule

The planned research schedule is heavily weighted on computational tasks. Bridgman will be the main high performance computer (HPC) utilized for analysis. Savio at UC-Berkley will be used to run Coeus for ETA-2 and ETA-SPNS. Due to the long nature of SAMPLER runs, the original ETA will be analyzed first on Bridgman. Figures 23 to 25 summarize a weekly schedule. The analysis periods are filled with many sub-tasks (plotting, χ^2, running into errors, ect.)

Figure 23. Research schedule part 1

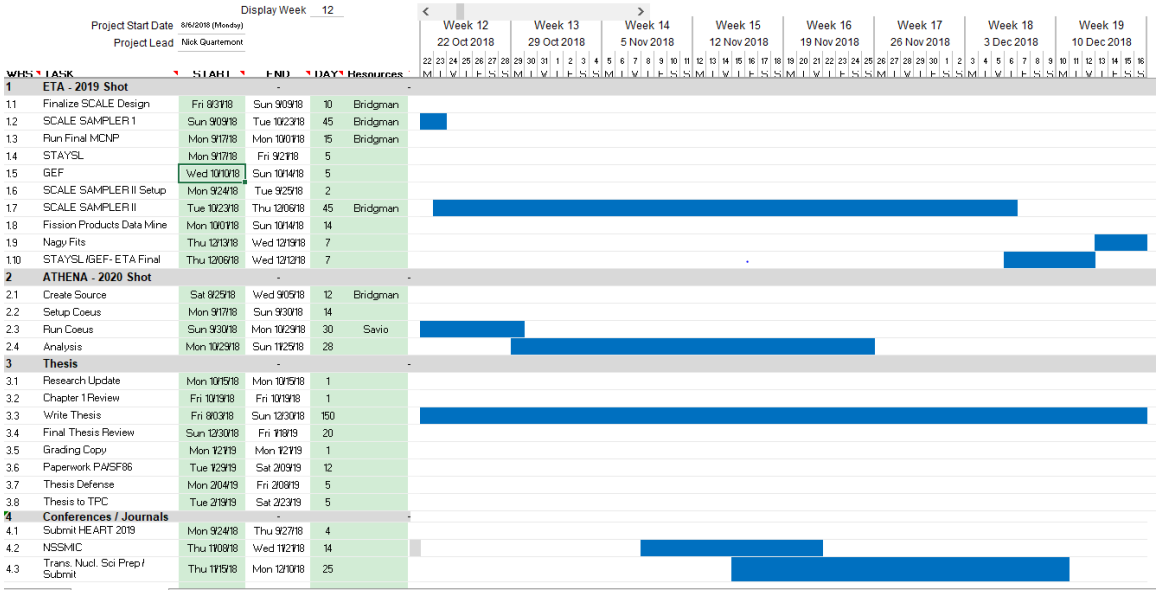

Figure 24. Research schedule part 2

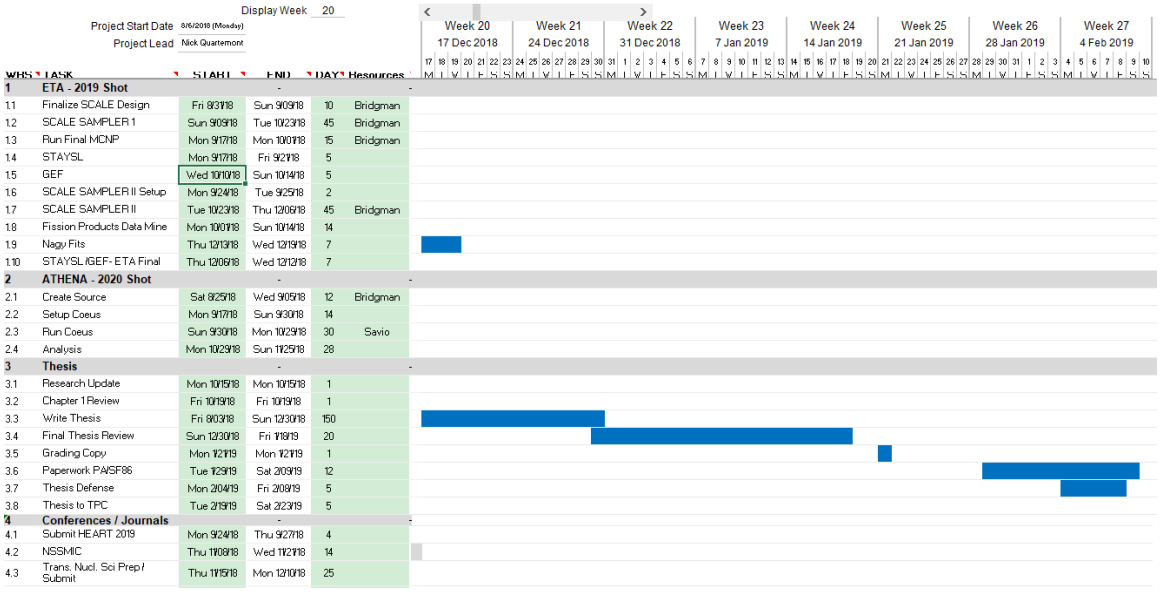

Figure 25. Research schedule part 3

5. Results

5.1 The Grading Copy

These are my results! I plan on presenting preliminary results at the brief, but they are not finished yet.

Bibliography

1. Office of the Secretary of Defense, "Nuclear Posture Review," 2018.

2. D. J. Trump, "State of the Union Address," 2018.

3. J. C. Martz, "Without Testing: Stockpile Stewardship in the Second Nuclear Age," Los Alamos National Lab.(LANL), Los Alamos, NM (United States), Tech. Rep., 2014.

4. Joint Defense Science Board/Threat Reduction Advisory Committee Task Force, "The Nuclear Weapons Effects National Enterprise," Office of the Under Secretary of Defense for Acquisition, Technology, and Logistics, Tech. Rep. June, 2010.

5. J. Bevins, "Targeted Modification of Neutron Energy Spectra for National Security Applications," Ph.D. dissertation, University of California, Berkeley, 2017.

6. C. J. Bridgman, *Introduction to the Physics of Nuclear Weapons Effects*. Fort Belvoir, VA: Defense Threat Reduction Agency, 2001.

7. K. P. Carney, M. R. Finck, C. A. McGrath, L. R. Martin, and R. R. Lewis, "The Development of Radioactive Glass Surrogates for Fallout Debris," *Journal of Radioanalytical and Nuclear Chemistry*, vol. 299, no. 1, pp. 363–372, 2014.

8. F. Dietrich and J. Escher, "Compound-nuclear Reaction Cross Sections via Surrogate Reactions," *Nuclear Physics A*, vol. 787, no. 1, pp. 237 – 242, 2007, proceedings of the Ninth International Conference on Nucleus-Nucleus Collisions.

9. N. D. Scielzo, J. E. Escher, J. M. Allmond, M. S. Basunia, C. W. Beausang, L. A. Bernstein, D. L. Bleuel, J. T. Burke, R. M. Clark, F. S. Dietrich, P. Fallon, J. Gibelin, B. L. Goldblum, S. R. Lesher, M. A. McMahan, E. B. Norman, L. Phair, E. Rodriguez-Vieitez, S. A. Sheets, I. J. Thompson, and M. Wiedeking, "Statistical γ Rays in the Analysis of Surrogate Nuclear Reactions," *Physical Review C - Nuclear Physics*, vol. 85, no. 5, 2012.

10. N. Gharibyan, "Development af a fission-proxy method for the measurement of 14-mev neutron fission yields at cams."

11. J. E. Escher, J. T. Burke, F. S. Dietrich, N. D. Scielzo, I. J. Thompson, and W. Younes, "Compound-nuclear reaction cross sections from surrogate measurements," *Rev. Mod. Phys.*, vol. 84, pp. 353–397, Mar 2012.

12. N. Galy, N. Toulhoat, N. Moncoffre, Y. Pipon, N. Bérerd, M. R. Ammar, P. Simon, D. Deldicque, and P. Sainsot, "Ion Irradiation Used as Surrogate of Neutron Irradiation in Graphite: Consequences on 14C and 36Cl Behavior and Structural Evolution," *Journal of Nuclear Materials*, vol. 502, pp. 20–29, 2018.

13. J. Bouchard and R. Heaphy, "QASPR Validation : Moving from Research Codes to Trusted Codes," Sandia National Laboratories, Tech. Rep., 2007.

14. Y. Kasesaz and M. Karimi, "A Novel Design of Beam Shaping Assembly to use D-T Neutron Henerator for BNCT," *Applied Radiation and Isotopes*, vol. 118, no. September, pp. 317–325, 2016.

15. I. M. Ardana and Y. Sardjono, "Optimization of a Neutron Beam Shaping Assembly Design for BNCT and Its Dosimetry Simulation Based on MCNPX," *Jurnal Teknologi Reaktor Nuklir Tri Dasa Mega*, vol. 19, no. 3, p. 121, 2017.

16. L. Zaidi, M. Belgaid, S. Taskaev, and R. Khelifi, "Beam Shaping Assembly Design of 7Li(p,n)7Be Neutron Source for Boron Neutron Capture Therapy of Deep-Seated Tumor," *Applied Radiation and Isotopes*, vol. 139, no. May, pp. 316–324, 2018.

17. J. E. Bevins, "Coeus V1.0," 2017. [Online]. Available: https://github.com/SlaybaughLab/Coeus/releases.

18. J. E. Bevins, S. Bogetic, L. A. Bernstein, R. Slaybaugh, and J. Vujic, "Metaheuristic Optimization Method for Neutron Spectra Shaping," *Transactions of the American Nuclear Society*, vol. 118, pp. 455–458, 2018.

19. R. Stickney, Jason, "Pulse Height Spectra Analysis of a Neutron Energy Tuning Assembly," Ph.D. dissertation, Air Force Institute of Technology, 2018.

20. Department of Defense, "Nuclear Weapons Technology," in *Military Critical Technologies List*, 1998.

21. S. Glasstone and P. J. Dolan, *The Effects of Nuclear Weapons*, 3rd ed. Washington D.C.: United States Department Of Defense, 1977.

22. K. H. Schmidt, B. Jurado, C. Amouroux, and C. Schmitt, "General Description of Fission Observables: GEF Model Code," *Nuclear Data Sheets*, vol. 131, no. May, pp. 107–221, 2016.

23. S. Nagy, K. F. Flynn, J. E. Gindler, J. W. Meadows, and L. E. Glendenin, "Mass Distributions in Monoenergetic-Neutron-Induced Fission of U238," *Physical Review C*, vol. 17, no. 1, pp. 163–171, 1978.

24. L. Greenwood and C. Johnson, "Least-Squares Neutron Spectral Adjustment with STAYSL PNNL," *EPJ Web of Conferences*, vol. 106, p. 07001, 2016. [Online]. Available: http://www.epj-conferences.org/10.1051/epjconf/201610607001

25. B. Rearden, M. Jessee, and Eds., *User Guide for the STAYSL PNNL Suite of Software Tools*, PNNL-22253, Pacific Northwest National Laboratory, Richland, WA, February 2013.

26. J. Duderstadt and L. Hamilton, *Nuclear Reactor Analysis*. New York: Jon Wiley & Sons, 1976.

27. J. Turner, *Atoms, Radiation, and Radiation Protection*. Oak Ridge, TN: Wiley, 2008.

28. M. Chadwick and E. Al., "ENDF/B-VII.1 Nuclear Data for Science and Technology: Cross Sections, Covariances , Fission Product Yield," *Nucl.Data Sheets*, vol. 112, no. 12, pp. 2887–2996, 2011.

29. K. Krane, *Introductory Nuclear Physics*. New York: Jon Wiley & Sons, 1988.

30. G. F. Knoll, *Radiation Detection and Measurement, 4th Edition.* Ann Arbor, MI: Wiley, 2010.

31. H. Salmon, R. nal, B. Oruncak, U. Akcaalan, and H. A. Yalim, "(n,2n) and (n,3n) Neutron Induced Reaction Cross Sections above 8 MeV," *Acta Physica Polonica, A*, vol. 128, no. 2B, pp. B–231 – B–235, 2015.

32. C. Tonchev, A and Stoyer, M and Becker, J and Macri, R and Ryan, , T. and Sheets, S and Gooden, M and Arnold, C and Bond, E and Bredeweg, , W. Fowler, M and Rusev, G and Vieira, D and Wilhelmy, J and Tornow, , J. Howell, C and Bhatia, C and Bhike, M and Krishichayan, F and Kelley, and S. Fallin, B and Finch, "Energy Evolution of the Fission-Product Yields from Neutron-Induced Fission of 235U, 238U, and 239Pu: An Unexpected Observation," in *The 6th International Conference on "Fission and Properties of Neutron-Rich Nuclei*, 2016.

33. J. Randrup and R. Vogt, "Nuclear Fission." in *LLNL-BOOK-591732*. Lawrence Livermore National Laboratory, 2012.

34. K.-H. Schmidt and B. Jurado, "General Description of Fission Observables," *JEFF Report 24*, 2014.

35. A. Nichols, D. Aldama, and M. Verpelli, "HANDBOOK OF NUCLEAR DATA FOR SAFEGUARDS: DATABASE EXTENSIONS," International Atomic Energy Agency, Tech. Rep. August, 2008.

36. M. James, R. Mills, and D. Weaver, "A new evaluation of fission product yields and the production of a new library (ukfy2) of independent and cumulative yields." *Progress in Nuclear Energy*, vol. 26, no. 1, pp. 1 – 29, 1991.

37. E. Privas, G. Noguere, J. Tommasi, C. De Saint Jean, K.-H. Schmidt, and R. Mills, "Measurements of the Effective Cumulative Fission Yields of 143 Nd, 145 Nd, 146 Nd, 148 Nd and 150 Nd for 235 U in the PHENIX Fast Reactor," *EPJ Nuclear Sciences & Technologies*, vol. 2, no. 32, pp. 1–16, 2016.

38. B. Singh, "Nuclear data sheets for a = 89," *Nuclear Data Sheets*, vol. 114, no. 1, pp. 1 – 208, 2013.

39. D. A. Brown, E. A. Mccutchan, M. W. Herman, S. Hoblit, G. P. A. Nobre, and B. Pritychenko, "Uncertainty Quantification in the Nuclear Data Program," *J. Phys. G: Nucl. Part. Phys.*, vol. 42, no. 034020, 2015.

40. F. Bostelmann and G. Strydom, "Nuclear Data Uncertainty and Sensitivity Analysis of the VHTRC Benchmark Using SCALE," *Annals of Nuclear Energy*, vol. 110, pp. 317–329, 2017.

41. A. Knecht, R. Hong, D. W. Zumwalt, B. G. Delbridge, A. Garcia, P. Mueller, H. E. Swanson, I. S. Towner, S. Utsuno, W. Williams, and C. Wrede, "Precision Measurement of the 6He Half-Life and the Weak Axial Current in Nuclei,," *Phys. Rev. Lett.*, vol. 108, no. 122502, 2012.

42. R. Capote, K. Zolotarev, V. Pronyaev, and A. Trkov, "International Reactor Dosimetry and Fusion File IRDFF v.1.05," *J. ASTM International*, vol. 9, no. 4, April 2012.

43. L. Greenwood, M. Kostal, S. Simakov, and A. Trkov, "Testing and Improving the International Reactor Dosimetry and Fusion File (IRDFF)," 2017.

44. K. I. Zolotarev and P. K. Zolotarev, "Evaluation of Some (n,n'), (n,γ), (n,p), (n,2n) AND (n,3n) Reaction Excitation Functions for Fission and Fusion Reactor Dosimetry Applications," INDC International Nuclear Data Committee, Tech. Rep. INDC(NDS)-0657, 2013.

45. N. P. Luciano, "A High-Energy Neutron Flux Spectra Measurement Method for the Spallation Neutron Source," Master's thesis, University of Tenessee Knoxville, 2012.

46. E. E. Lewis and W. F. Millar Jr, *Computational Methods of Neutron Transport*. New York: John Wiley & Sons, 1984.

47. L. Kuijpers, R. Herzing, P. Cloth, D. Filges, and R. Hecker, "On the Determination of Fast Neutron Spectra with Activation Techniques; its Application in a Fusion Reactor Blanket Model," *Nuclear Instruments and Methods*, vol. 144, no. 2, pp. 215–224, 1977.

48. E. Vagena, K. Theodorou, and S. Stoulos, "Thick-foils Activation Technique for Neutron Spectrum Unfolding with the MINUIT RoutineComparison with GEANT4 Simulations," *Nuclear Instruments and Methods in Physics Research, Section A: Accelerators, Spectrometers, Detectors and Associated Equipment*, vol. 887, no. January, pp. 64–69, 2018.

49. M. Reginatto, "Overview of Spectral Unfolding Techniques and Uncertainty Estimation," *Radiation Measurements*, vol. 45, no. 10, pp. 1323–1329, 2010.

50. F. G. Perey, *Least-Squares Dosimetry Unfolding: The Program STAY'SL (ORNL/TM-6062)*, Oak Ridge, Tennessee, 1977.

51. H. R. Vega Carrillo and M. P. I. De La Torre, "Catalogue to select the initial guess spectrum during unfolding," *Nuclear Instruments and Methods in Physics Research, Section A: Accelerators, Spectrometers, Detectors and Associated Equipment*, vol. 476, no. 1-2, pp. 270–272, 2002.

52. B. Rearden, M. Jessee, and Eds., *SCALE Code System*, ORNL/TM-2005/39 ,Version 6.2.3, Oak Ridge National Laboratory, Oak Ridge Tennessee, March 2018, available from Radiation Safety Information Computational Center as CCC-834.

53. M. J. Wang, R. J. Sheu, J. J. Peir, and J. H. Liang, "Criticality Calculations of the HTR-10 Pebble-bed Reactor with SCALE6/CSAS6 and MCNP5," *Annals of Nuclear Energy*, vol. 64, pp. 1–7, 2014.

54. S. R. Johnson and K. T. Clarno, "Comparison of SCALE and MCNP Results for Computational Pebble Bed Benchmarks," *Trans.\ Am.\ Nucl.\ Soc.*, vol. 96, no. April, pp. 420–422, 2007.

55. Y. F. Chen, R. J. Sheu, S. H. Jiang, J. N. Wang, and U. T. Lin, "Surface Dose Rate Calculations of a Spent-Fuel Storage Cask by Using MAVRIC and Its Comparison with SAS4 and MCNP," *Nuclear Technology*, vol. 175, no. 1, pp. 343–350, 2011.

56. K.-h. Schmidt, B. Jurado, C. Amouroux, C. Schmitt, C. I. N. P, C. S. B. P, and F. Gradignan, "General Description of Observables in Low-energy Fission : GEF Model Code," 2015.

57. J. R. Taylor, *An Introduction to Error Analysis: The Study of Uncertainties in Physical Measurements*, 2nd ed. South Orange, NJ: University Science Books, 1997.